THE UNIVERSITY OF MICHIGAN
COLLEGE OF LITERATURE SCIENCE AND THE ARTS
Department of Physics

Technical Report No. 28

π^-p ELASTIC SCATTERING AT 180 DEGREES FROM 1.6 TO 5.3 GeV/c

Stephen W. Kormanyos

ORA Project 03106

under contract with:

DEPARTMENT OF THE NAVY
OFFICE OF NAVAL RESEARCH
WASHINGTON, D.C.

CONTRACT NO. Nonr-1224(23)
NR-022-274

administered through:

OFFICE OF RESEARCH ADMINISTRATION ANN ARBOR

April 1967

This report was also a dissertation submitted in partial fulfillment of the requirements for the degree of Doctor of Philosophy in The University of Michigan, 1966.

TABLE OF CONTENTS

LIST OF TABLES

LIST OF FIGURES

ABSTRACT

We have measured the differential cross section for π^-p elastic scattering at 180° in steps of 0.10 GeV/c or less in the region from 1.6 to 5.3 GeV/c.

There is considerable structure in the cross section. This may be interpreted as an interference effect between the resonance amplitude and the non-resonant or background amplitude.

There is a dramatic destructive interference at $P_0 = 2.15$ GeV/c. which is quite interesting as the cross section drops almost two orders of magnitude in this region.

Another interesting feature of the experiment is the large narrow peak in the cross section at $P_0 = 5.12$ GeV/c. We believe that this is firm evidence for the existence of a nucleon resonance with a mass of (3245 $\pm$ 10) MeV. This N* (3245) has a full width at half-maximum of less than 35 MeV. The width of the resonance is about 1% of its mass.

Parities and the quantity $X(J + 1/2)$ are given for various N* resonances where X is the elasticity and J is the spin of the resonance.

I. INTRODUCTION

In recent years many high energy physics experiments have been done to investigate the existence and properties of resonances. Traditionally the mass, width, and isotopic spin have been investigated in total cross section measurements. The resonances yield structure in the total cross section and from this structure some properties of the resonances can be learned. The spin and parity has been studied in angular distributions.

In this experiment we have employed a different technique to measure the properties of the N* resonances. We measured the differential cross section at 180° as a function of energy. Because of the interference of the resonances with the background, quite a bit of structure was present in the cross section. From our data we were able to determine the parities and the quantity $X(J+1/2)$ (where X is the elasticity and J is the spin of the resonance) for various N* resonances. This method of probing resonances appears to be more sensitive than looking for bumps in the total cross section.

We have measured the differential cross section for $\pi^- p$ elastic scattering at 180° in steps of 0.10 GeV/c or less in the region from 1.6 to 5.3 GeV/c. This experiment was done at Argonne National Laboratory on the Zero Gradient Synchrotron.

The differential cross section for $\pi^- p$ elastic scattering in the backward hemisphere has been measured by other experimenters. However, none of them has taken measurements as far back as 180°. Our data agrees with other experiments having measurements near 180°.[1-7]

There is considerable structure in the cross section. This may be interpreted as an interference effect between the resonance amplitude and the non-resonant or background amplitude.

There is a dramatic destructive interference at P_o = 2.15 GeV/c which is quite interesting as the cross section drops almost two orders of magnitude in this region.

Another interesting feature of the experiment is the large narrow peak in the cross section at P_o = 5.12 GeV/c. We believe that this is firm evidence for the existence of a nucleon resonance with a mass of (3245 $\pm$ 10) Mev. This N* (3245) has a full width at half-maximum of less than 35 MeV. The width of the resonance is less than 1% of its mass. It seems remarkable that such a massive particle should be so stable. Assuming a smooth background amplitude we found the parities of various N* resonances. We also calculated the qunatity X(J + 1/2) for various N*'s where X is the elasticity and J is the spin of the resonance.

II. EXPERIMENTAL EQUIPMENT AND PROCEDURES

A. CIRCULATING PROTON BEAM AND INTERNAL TARGET

Figure 1 shows the beam layout. The 12.5 GeV/c circulating proton beam struck a 90% copper, 10% aluminum internal target 1/8" x 1/8" x 3.85" long with a beryllium lip. This internal target was a pop up type. During the acceleration cycle the target was out of the beam envelope. After the acceleration cycle the target moved up and the beam was brought onto the target.

The circulating proton beam made many passes through the internal target during the spill. For example the duration of a typical spill was 150 msec. The time for a proton to make one revolution was approximately 640 nsec. So in the spill time the beam made on the order of 235,000 passes through the target.

The circulating proton beam was brought onto the internal target during flat top by increasing the frequency of the accelerating voltage. This is called the radio frequency (RF). As the RF frequency increases the particles get out of step with it, lose momentum, move in a smaller circle and are thus brought onto the target. There was a feedback loop which kept the spill as constant as possible.

The internal target was placed at various positions from 3 to 5 feet back into the field of the ZGS ring magnet. Its position was determined by the selection of two parameters and the use of appropriate graphs given in ZGS Users Handbook. These two parameters were the pion production angle, which was zero or as close to zero as we could get in order to have maximum pion

production, and the pion momentum.

After the 3.5 GeV/c run we added a beryllium lip to the leading edge of the copper target in order to remove the sensitive dependence of targeting efficiency on the target angle. Measurements had indicated as much as a 15% decrease in beam counts for a 1% change in target angle. The thickness of the beryllium lip was sufficient to jump the circulating proton beam about 0.03 inches per pass through the lip.

The internal target coordinates were calculated before the experiment was run. During the experiment as we went to a new pion energy the internal target was moved to its appropriate position and angle. The internal target was mounted on a drive mechanism which moved it into our desired positions.

The reason for placing the target back into the ZGS ring magnet was to obtain zero degree pion production, that is maximum pion production, for most of our experiment. In addition, the ZGS ring magnet, which bent the pions produced at zero degrees through 17° into our beam line, selected negatively charged particles and also partially momentum analyzed these particles.

B. π BEAM INTENSITY

The π^- beam intensity was 3.5×10^5 pions per 5×10^{11} circulating protons in the region 2.0 to 4.0 GeV/c. At higher and lower momenta the intensity dropped off. At lower momenta more beam pions decayed while at higher momenta the pion production cross section decreased. Throughout most of the experiment we had intensities in the range of 1×10^5 to 3.5×10^5 pions per pulse.

In the course of the experiment the zero degree π^- production for 12.5

GeV/c protons on copper was measured. The results are given in the appendix.

C. π BEAM GEOMETRY

The pion beam line is shown in Figure 1. It consists of three quadrupole doublets for focusing and two bending magnets for momentum analysis. There is an intermediate focus at the second beam collimator and a second focus at the liquid hydrogen (LH_2) target. The beam had a momentum bite of $\Delta P/P = \pm 3/4\%$ and subtended a solid angle of 1×10^{-4} steradians at the internal ZGS target. This gave the beam particles an angular divergence of less than 3 milliradians at the target.

The beam bending magnets were 18 inches wide, 6 inches high, and 72 inches long. We calculated the currents needed by using graphs of central magnetic field versus current, supplied by the ZGS Users Handbook for these magnets.

The quadrupole magnets were 10 inches nominal diameter and 36 inches long. For the quadrupoles we also used magnetic field gradients versus current curves from the ZGS Users Handbook.

For the beam bending magnets we had symmetrical bending through 8.50°. That is with respect to the magnet axis $\theta_{initial} = \theta_{final} = 4.25°$. So then the magnetic field B_o was calculated from the equation:

$$B_o L_{eff} = 1313.22\ P(\sin \theta_{in} + \sin \theta_{out}) \qquad (1)$$

where B_o is in Kg., P in GeV/c, L_{eff} in inches.

For the values of the gradients we used an iterating beam design computer program. We specified the positions of our two beam foci, and intermediate focus at the 1" x 1" beam collimator and a second focus at the LH_2 target. We

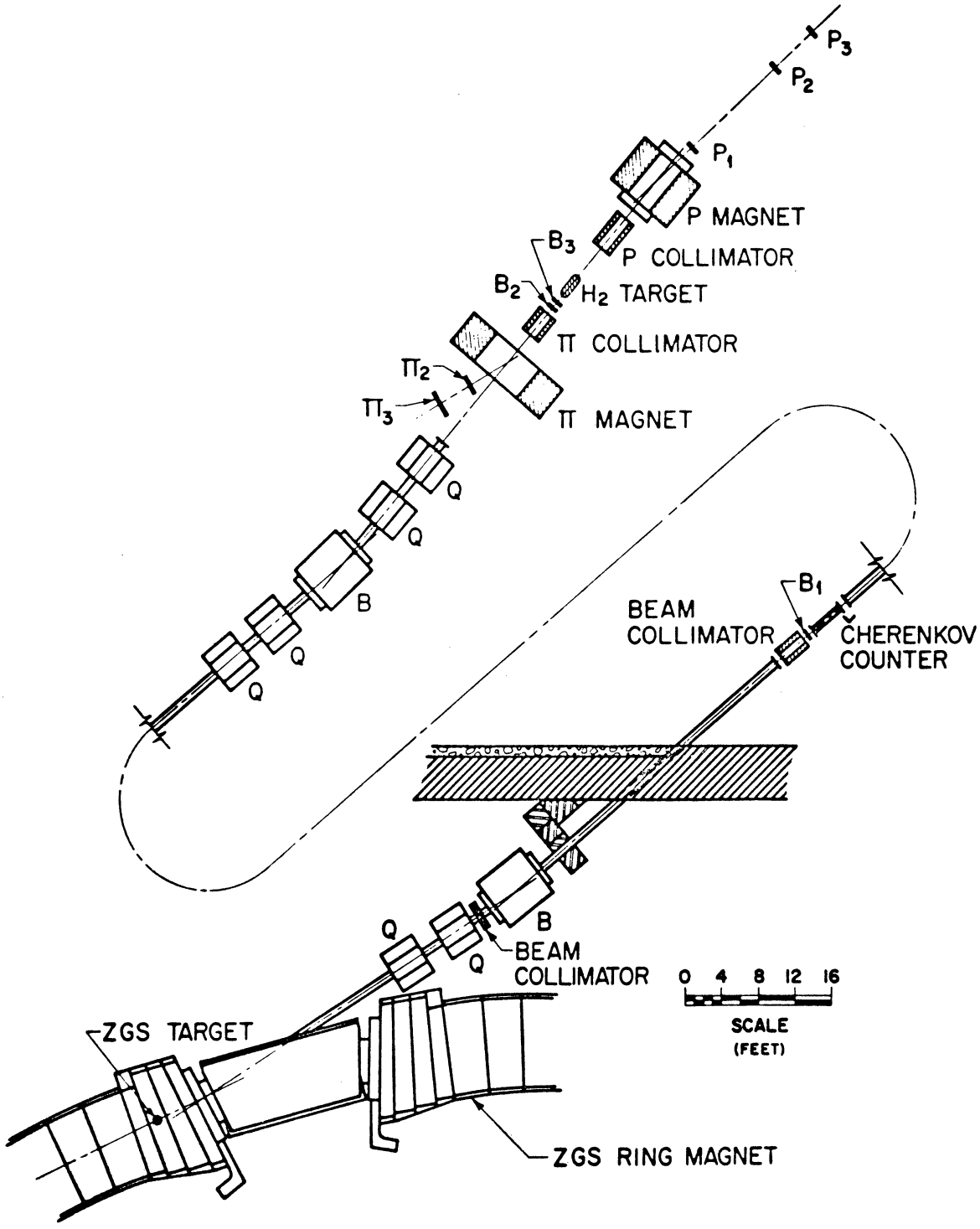

Figure 1. The beam layout.

selected the particle momentum, the orbit starting values, and the approximate values of the gradients. The program then iterated the gradients until our focal conditions were satisfied. By slightly varying our starting orbits and our initial gradients we arrived at a satisfactory focus and beam angular divergence at the LH_2 target. There was a solid angle beam collimator between the second quadrupole and the first bending magnet. Its dimensions were 3.5" wide, 4.5" high, and 24" long. We wanted as small a beam angular divergence as possible since we wished to study elastic scattering as close to 180° as possible. We settled on a beam which gave us an angular divergence of less than 3 milliradians. We worked out the beam design for 4.0 GeV/c and linearly scaled the other gradients from this value. At 4.0 GeV/c the beam profile is shown in Figure 2.

After passing through the permanent 17° beam magnets the incident π^- beam passed through the π-magnet which deflected it by 2.3 to 1.3 degrees onto the LH_2 target. The π magnet gap was 84" wide, 14" high, and 30" long. Its magnetic field integral was measured by a wire orbit technique.

D. π BEAM TUNING

At each new incident beam energy we tuned the beam. We had a beam monitor consisting of three small scintillation counters mounted on a stand which we placed on the outside of Q_1 inside the ZGS ring shielding. We counted the triples coincidences of these counters. This beam spill monitor output was directly proportional to the beam spill. In tuning we maximized the number of pions relative to this beam monitor. The number of pions coming down our beam line was determined by the coincidences between the three beam counters

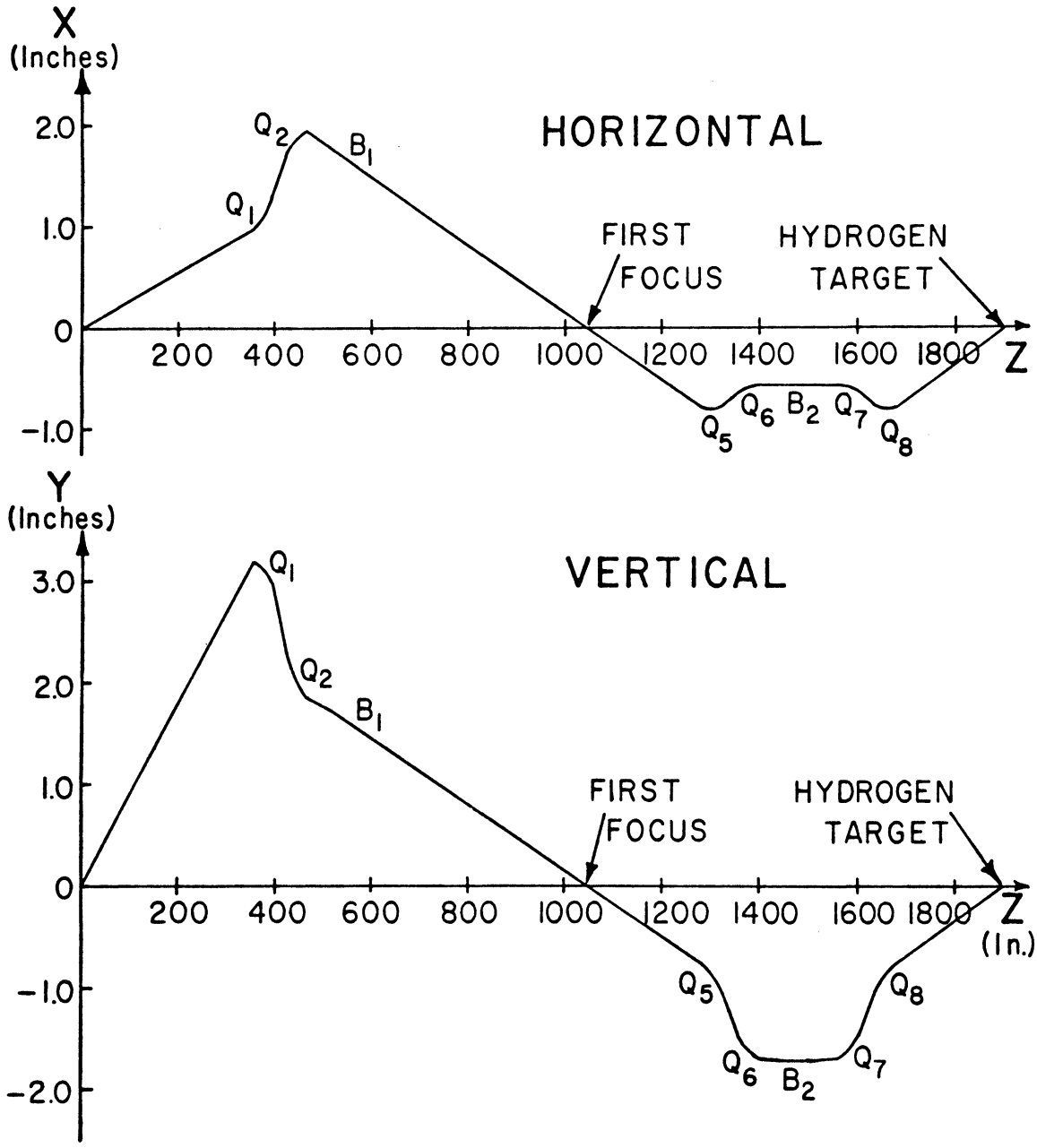

Figure 2. Pion beam profile

B_1, B_2, B_3, and the Cherenkov counter $\overset{v}{C}$. This quantity is denoted by $\overset{v}{BC}$.

In tuning we used a TSI Preset Count Control built by the ANL Electronics Division. This was connected to the monitor scalar. At a preset number of counts on the monitor scalar, say 10^5 or 10^6, the Preset Control would turn off all the scalars. With this the ratio $\overset{v}{BC}/M$ would be directly readable as M would be a power of 10 and no division was necessary. This was a great help in tuning.

In changing to a new energy the internal target was moved to a new position. The quadrupoles and bending magnets were set at their calculated values. The tuning was done as follows. First B_1 was tuned, then Q_1, Q_2, Q_6 and Q_7, Q_5 and Q_8, then B_1 was rechecked. Typical tuning curves are shown in Figures 3-5. B_2 was not tuned but was set and held at its calculated value. This magnet gave us our final momentum selection. The rest of the beam was tuned around B_2.

The central magnetic field of B_2 as a function of current or shunt voltage was measured with nuclear magnetic resonance techniques over the entire range of the values used in the experiment. Hysteresis was found to be negligible. By this measurement the laboratory momentum of the pion beam was known to $\pm$0.03 GeV/c.

E. HYDROGEN TARGET

The source of the target protons was a liquid hydrogen (LH_2) target. The cylindrical target was 12" long and 1-1/2" in diameter with its axis along the beam axis. The LH_2 target was carefully surveyed into position. During the course of the experiment the LH_2 target was moved and surveyed into a new

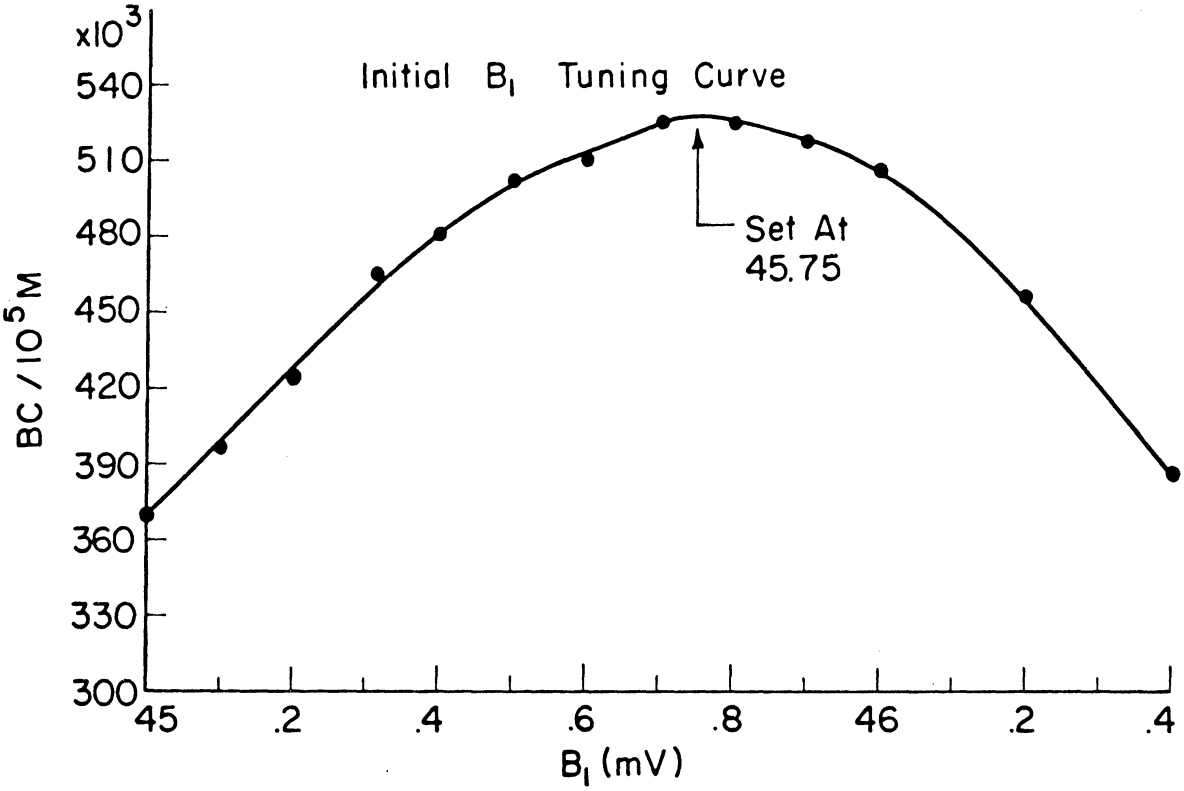

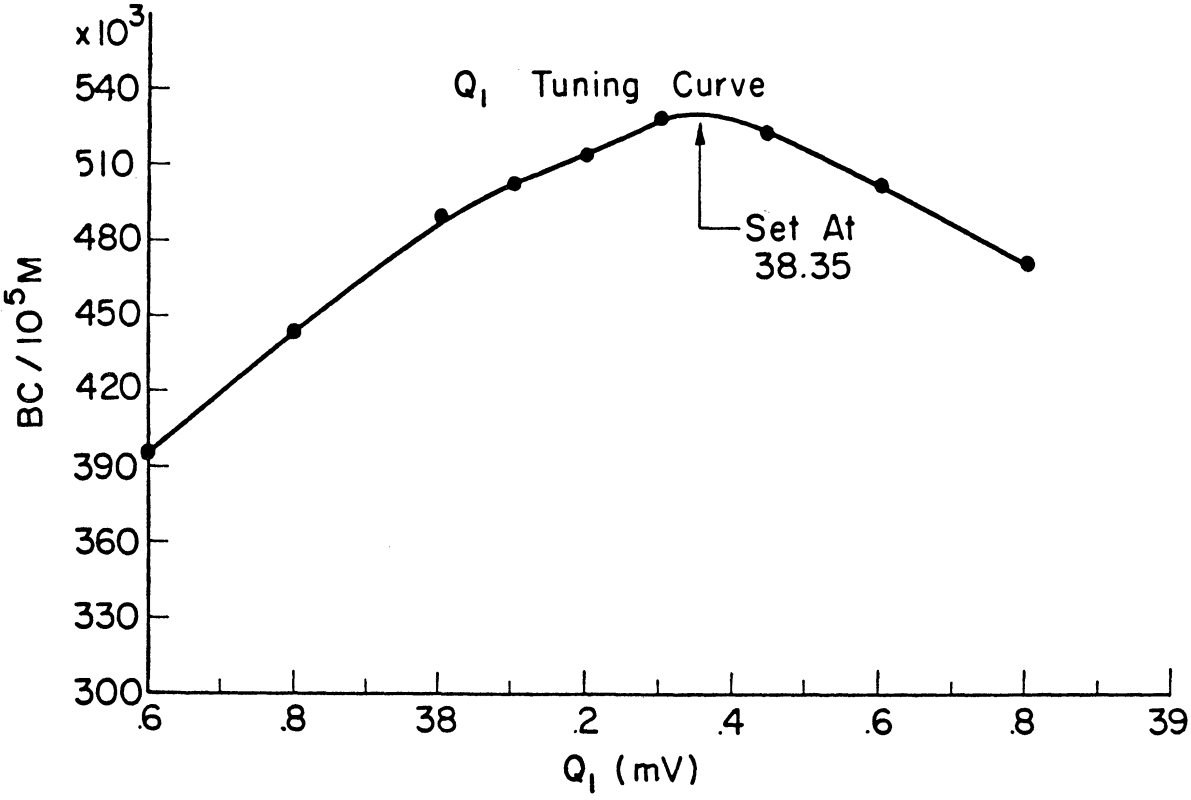

Figure 3. Q_1 and initial B_1 tuning curves.

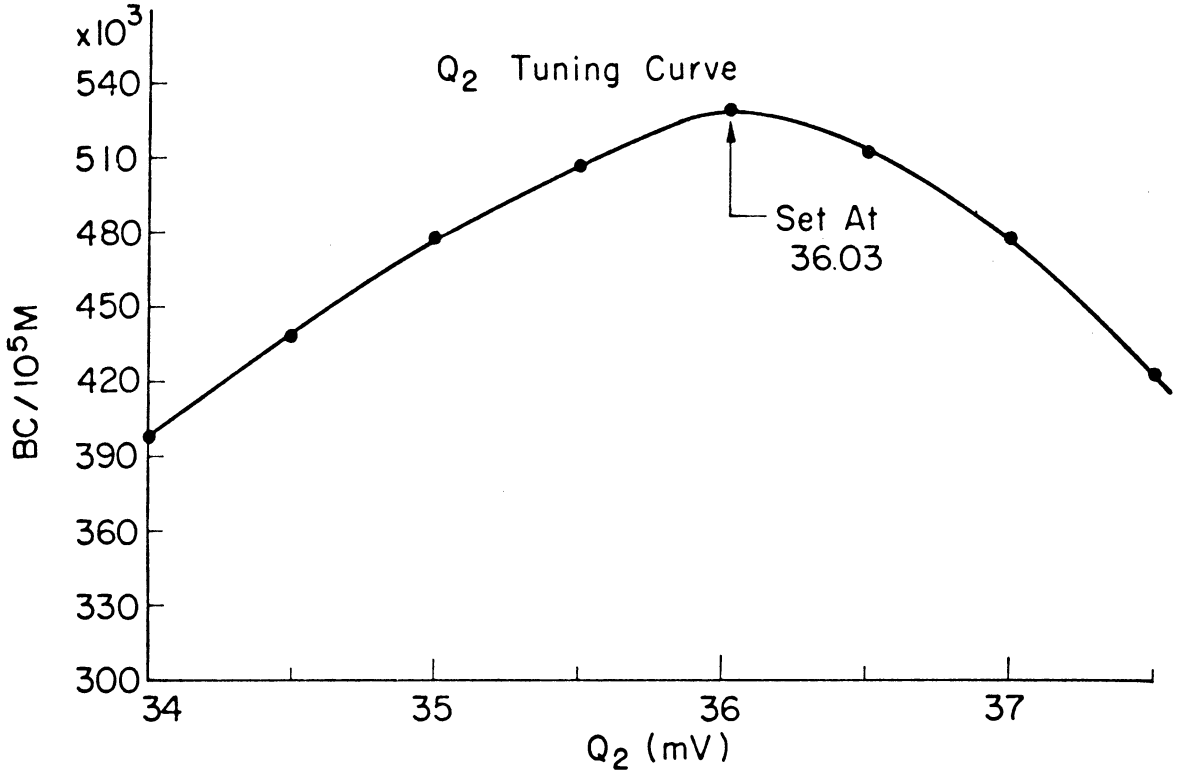

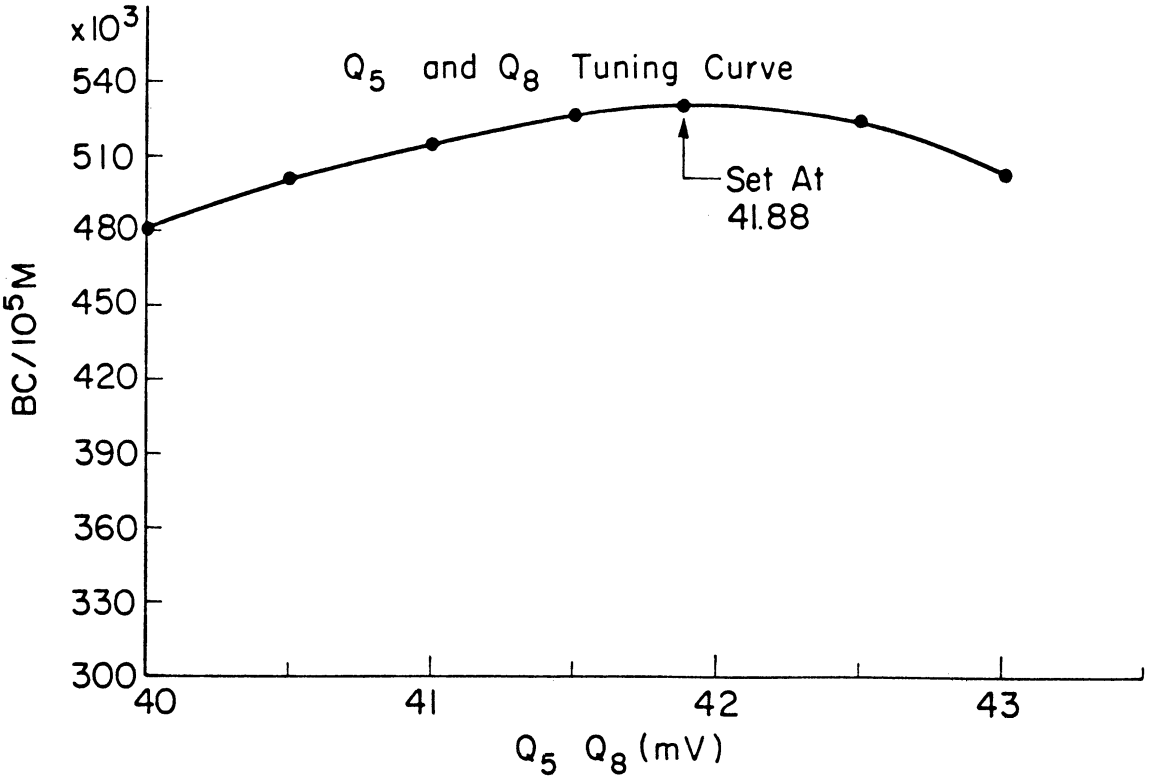

Figure 4. Q_2 and Q_5, Q_8 tunning curves.

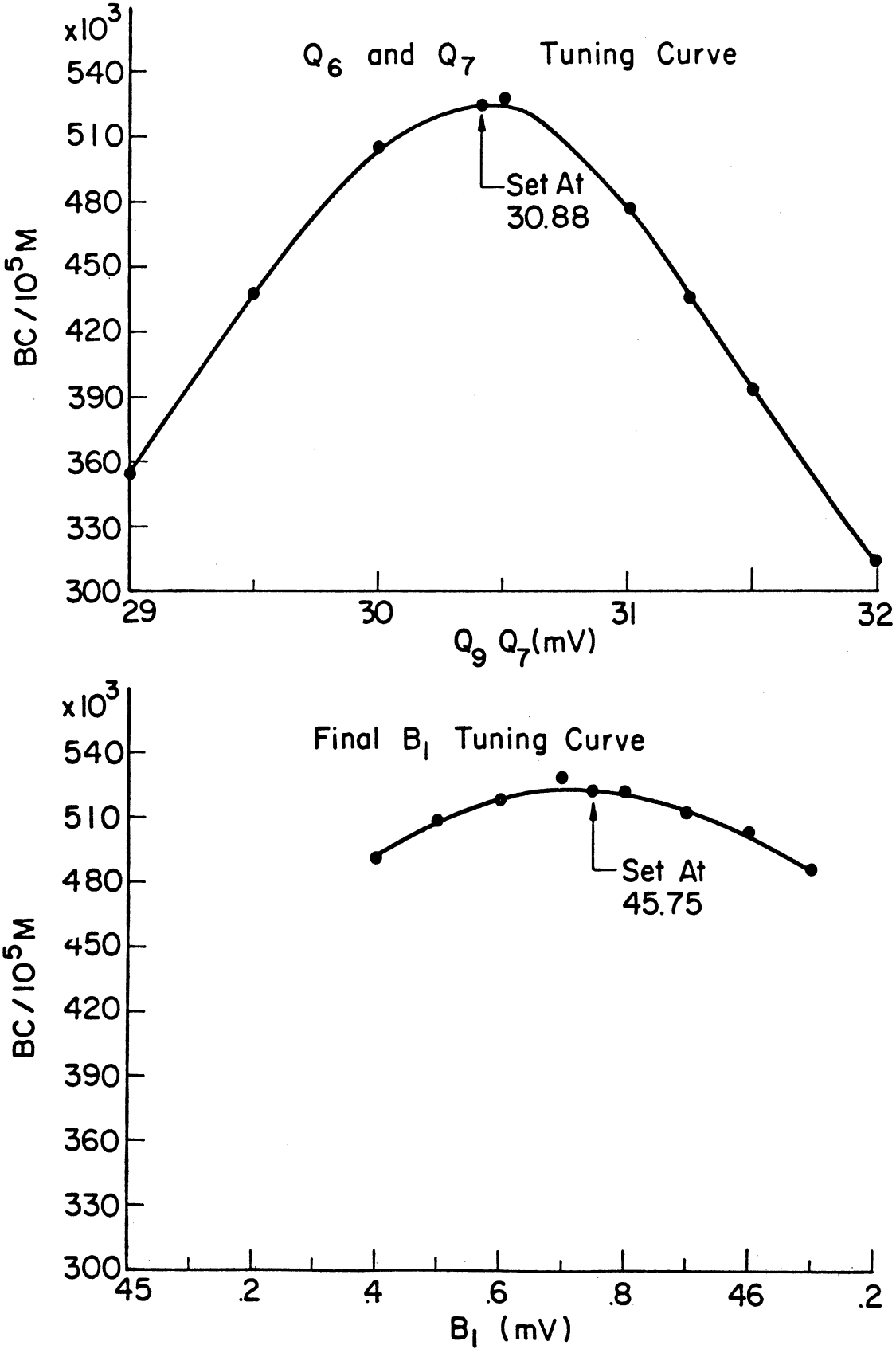

Figure 5. Q_6, Q_7 and final B_1 tuning curves.

position two more times, so that the scattered pions would not have to be bent through too large an angle. Thus in the experiment we had three beam "geometries." The experimental layout is shown in Figure 6. The LH_2 target is shown in Figure 7.

F. COUNTERS

The counters consisted of sheets of Pilot scintillator B with tapered lucite light pipes. These were cut and polished by the Pilot Chemicals Company. Both the scintillator and light pipe were wrapped with aluminum foil and black masking tape to give internal reflection without light leaks. The counter sizes are shown in Table I.

TABLE I

SCINTILLATION COUNTER SIZES

Counter	Size width x height (inches)	Thickness (inches)	Energy Range (GeV/c)
π_2	14 x 14	1/2	1.6 -5.3
π_3	16 x 16	1/2	1.6 -5.3
p_1	8 x 8	1/2	1.6 -2.5
	6 x 6	1/2	2.6 -5.3
p_2	12 x 12	1/2	1.6 -5.3
p_3	12 x 12	1/2	1.6 -3.15
	9 x 9	1/2	3.15-4.5
	8 x 8	1/2	4.5 -5.3
B_1	1 x 1	1/8	1.6 -5.3
B_2, B_3	1 inch in diameter	1/8	1.6 -5.3

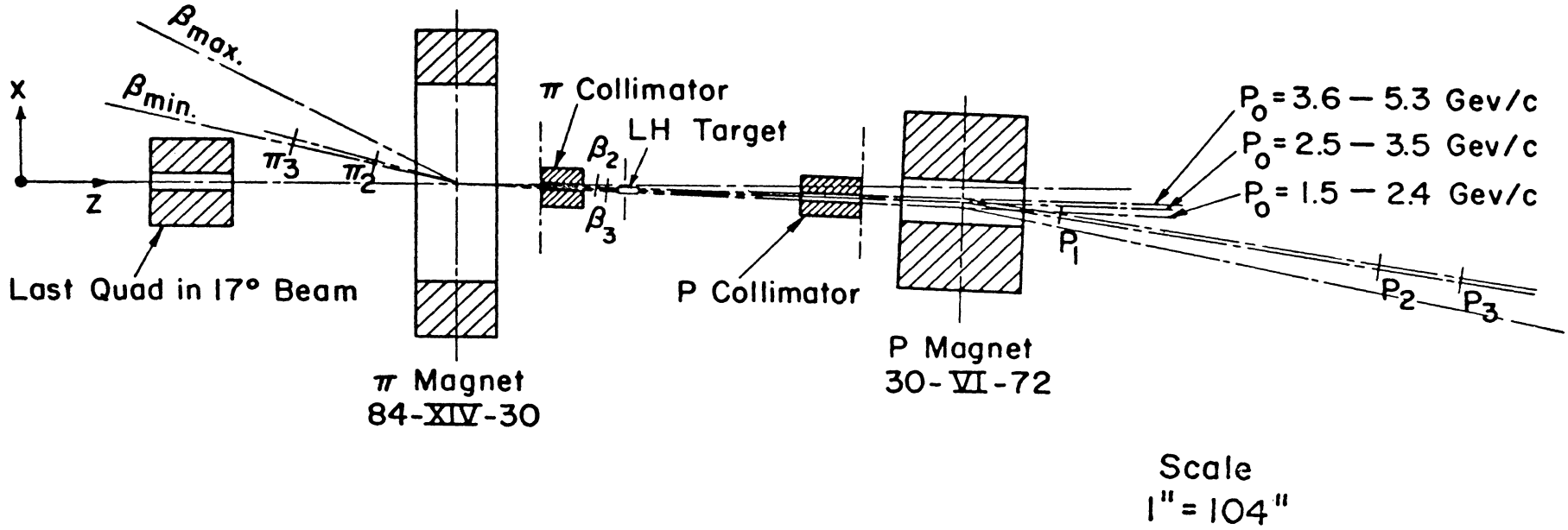

Figure 6. Layout of π^-p elastic scattering at 180°.

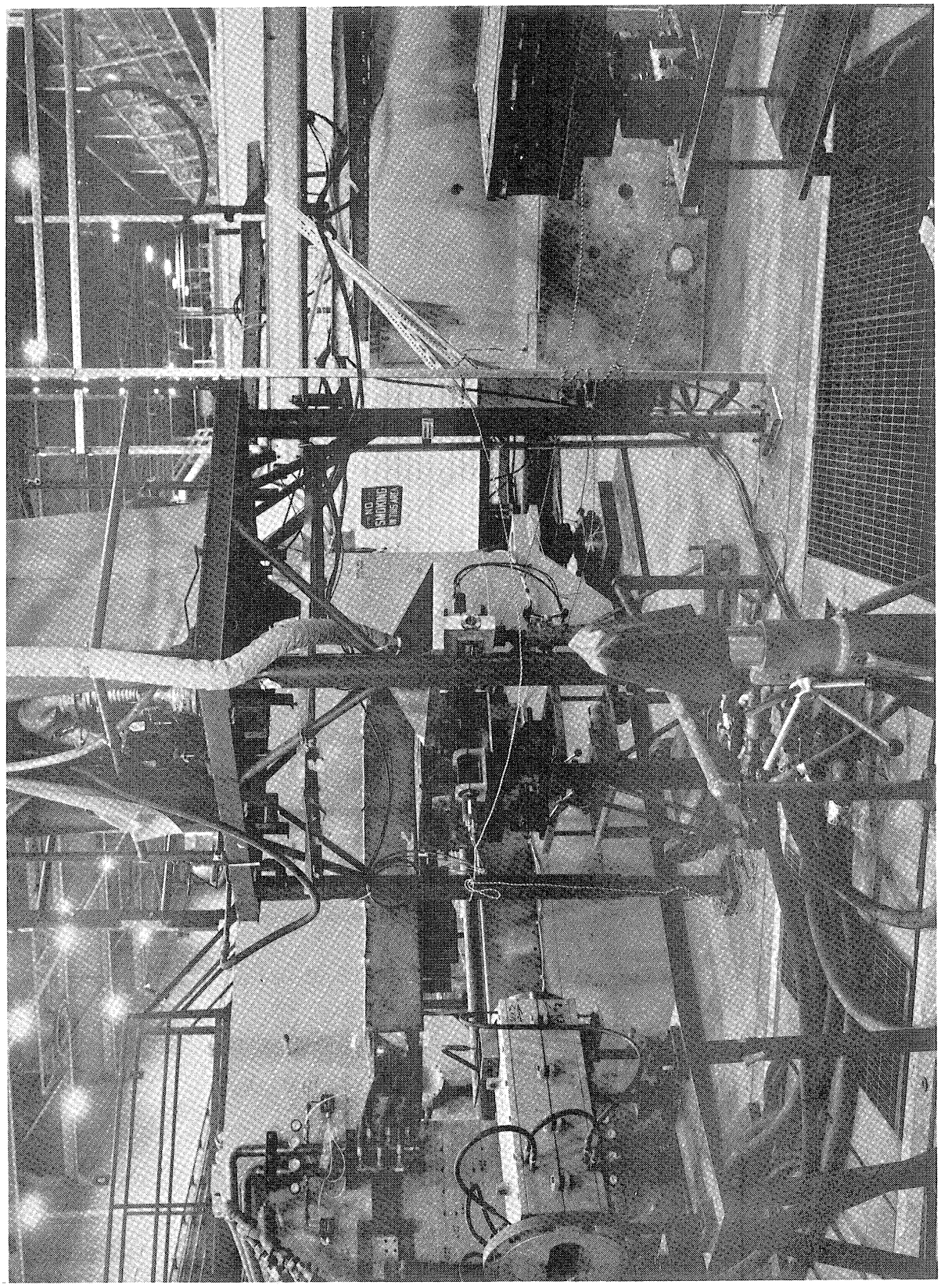

Figure 7. The hydrogen target.

The light pipes were optically connected to RCA 7746 photomultiplier tubes. These are fast 10 stage tubes. The time between the light pulse and the voltage pulse was stable to less than a nanosecond. The rise time itself was about 2 nanoseconds, but by triggering on the rising edge of the voltage pulse we got stability of better than one nanosecond. The tubes were encased in Mu-metal shields to eliminate stray magnetic fields. The anode voltage on each tube was set by running a high voltage curve and setting the voltage about 150 volts above the knee of the plateau as shown in Figure 11.

The phototube bases were Model 531 S manufactured by Nanosecond Systems. Because of the high counting rate, the bases of the beam counters were modified so that the voltage would remain more stable when a large current was being drawn.

The wavelength of the maximum light output of the Pilot Scintillator B is 4000 Anstroms and at this wavelength the relative sensitivity of the RCA 7746 photomultiplier is 90%.

The counters were attached to lateral adjusters and then mounted on transit stands. In this manner they were very stable and could quite easily be positioned very accurately. By means of a plumb bob hung over the center of the counters they could be horizontally positioned with respect to survey lines laid out by the Argonne survey crew. Vertical positioning was done using a transit. A view of the π counters is shown in Figure 8.

Since the refractive index of the scintillator is 1.58 light transit times from one end of the scintillator to the other of about one or two nanoseconds could be expected. The resolving time was improved by having all

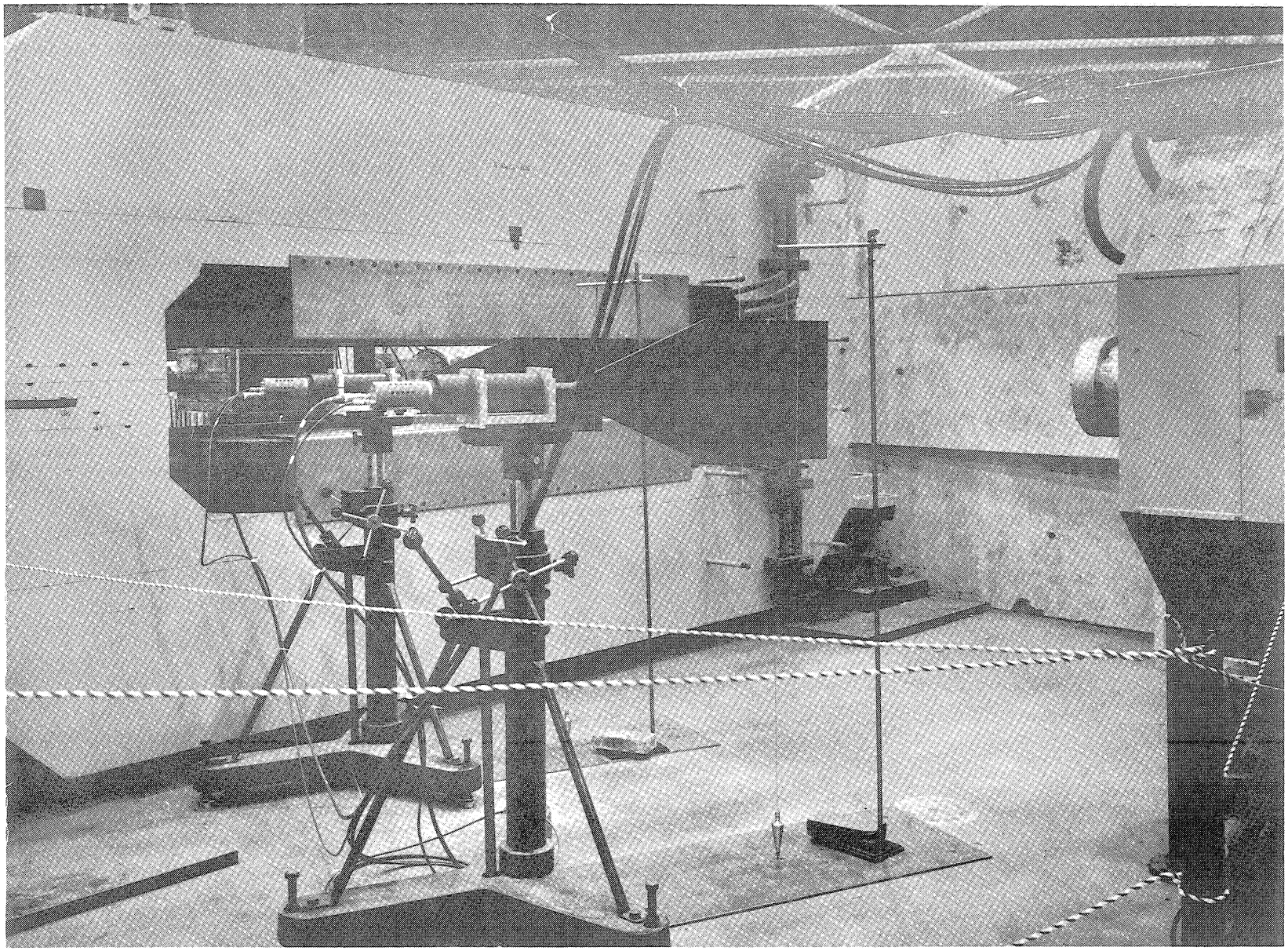

Figure 8. The π_2 and π_3 counters.

the counters in a telescope pointing in one direction so that the particle then passed through the same part of each counter and the light transit time was approximately equal for each counter.

To further improve resolution, since we were accepting scattering angles in a small range about 180°, the counters in the p telescope all pointed toward + x while the counters in the π telescope all pointed toward -x. By doing this the light transit time of both the π and p telescopes can be made approximately equal. The two beam counters B_2 and B_3 were pointed in opposite directions with overlapping scintillators so that the pions would have to go through both scintillators in order to be counted. This was done because had the counters pointed in the same direction, pions could have gone through both light pipes, given off Cherenkov light, been counted as a beam pion, and yet miss the LH_2 target.

G. SCATTERING ANALYSIS

We have an incident π^- beam elastically scattered from protons in a LH_2 target. This elastic scattering has five independent variables: P_{inc} the incident laboratory momentum of the π^-, P_π and P_p the final laboratory momenta of the π and p after scattering, and θ_π and θ_p the laboratory angles of the π and p. Conservation of energy and momentum give us three constraints

$$P_\pi \sin \theta_\pi = P_p \sin \theta_p$$

$$P_{inc} = P_\pi \cos \theta_\pi + P_p \cos \theta_p \qquad (2)$$

$$m_p + (P_{inc} + m_\pi^2)^{1/2} = (P_p^2 + m_p^2)^{1/2} + (P_\pi^2 + m_\pi^2)^{1/2}$$

For 180° scattering these reduce to

$$\frac{P_\pi}{P_p} = \left(\frac{J_p}{J_\pi}\right)^{1/2} \quad \text{where} \quad J_i = \frac{d\Omega_i^{LAB}}{d\Omega_i^{CM}} \tag{3}$$

$$P_{inc} = P_p - P_\pi$$

$$m_p + (P_{inc}^2 + m_\pi^2)^{1/2} = (P_p^2 + m_p^2)^{1/2} + (P_\pi^2 + m_\pi^2)^{1/2} .$$

So there remain only two independent variables. One of the strong points of our system is that we experimentally determine all five quantities and thus have three constraints on the system in addition to coplanarity.

We detected and counted the incident beam pions, the 180° backscattered π and the 0° forward scattered p. We counted incident beam particles with scintillation counters B_1, B_2, and B_3 in coincidence with a gas threshold Cherenkov counter containing 80-140 psig of ethane. This beam coincidence will be referred to as $B\check{C}$. The Cherenkov counter discriminated against antiprotons and K's which comprised less than 1% of the beam. As we increased the energy we decreased the Cherenkov pressure so that we would discriminate against K's. See Figure 13. The first counter B_1, at the first focus was a 1" square-1/8" thick counter. The beam counters B_2 and B_3 were 1" diameter by 1/8" thick circular counters.

The liquid H_2 target was 12" long by 1-1/2" in diameter. However, the interaction region was defined by the 1" diameter circular beam counters (B_2, B_3). With this arrangement we were sure that the detected incident beam particles did indeed impinge on the LH_2 in the target. By visual observation it was seen that the mylar bag containing the LH_2 was never completely full

of LH_2. There was approximately a 1/8" space at the top which did not fill with LH_2.

Our detection system for the scattered particles was a double spectrometer, a π arm, and a p arm, in coincidence. Let us now follow an elastic scattering event. The incident π passes through the π magnet and is bent through a small angle depending on the geometry in use, passes through the π collimator, through B_2 and B_3 beam counters and then into the LH_2 target. We were interested in 180° elastic scattering. After such a scattering the backward scattered π passed through the π magnet in the opposite direction to the beam and was deflected so as to pass through the π telescope counters π_2 and π_3. Thus the scattered π was cleanly separated from the incident π beam. The forward scattered proton passed through the p magnet which deflected it through the p telescope counters p_1, p_2, p_3.

The π^- particles which did not interact, the great majority of the beam, being of opposite electrical charge to the protons, were bent in the opposite direction. In this way the scattered protons were also cleanly separated from the non-interacting π^- beam.

The incident and scattered pions passed through the π collimator while the scattered proton passed through the p collimator. These collimators were considerably oversized so that the scintillation counters rather than the collimators would define the solid angle. The collimators were made of accurately machined steel plates surrounded by lead bricks supported on adjustable steel tables.

The p-magnet was a standard bending magnet (18 VI 72). The π-magnet was

a large gap bending magnet 30" long, 14" high, and 84" wide. The momentum bite of the π telescope was about $\Delta P/P = \pm 30\%$, while for the p telescope $\Delta P/P$ was about $\pm 10\%$. The term momentum bite in the above means how much the momentum of the particle under consideration can very and still pass through its telescope. The current settings in the π p magnets and the counter telescope angles were determined as follows.

For a given geometry and incident beam momentum the magnetic field integral for the π-magnet necessary to bring the incident π^- beam onto the LH_2 target was calculated via the equation

$$P(\sin\theta_{IN} + \sin\theta_{OUT}) = \frac{\int \vec{B} \cdot d\vec{l}}{1313.22} .$$

Once the field integral was calculated the angle of the π telescope was fixed as the momentum of the backscattered π^- was determined by kinematics.

The magnetic field of the p-magnet was adjusted so that the forward scattered p would be bent into the proton telescope and at the same time cleanly separated from the negatively charged π^- beam.

An advantage of the experiment was that in going from one energy to the next higher one in the same geometry only small changes were made in the system. This was because P_π was close to 0.400 GeV/c throughout the experiment. As we went to a higher energy the current in the π magnet was increased so that the higher momentum incident beam still passed through the LH_2 target. The current in the p magnet was increased so that the higher momentum protons still passed through the p telescope. The only physical change in going from one incident momentum to the next was to increase the π telescope angle

by about 1°. This consisted of moving the two π counters by about one inch. Also small timing changes were made due to the difference in time of flight of the π and p.

Not having to move the LH_2 target, the magnets, or the p counters removed possible systematic errors to misalignment.

The solid angle subtended in the center of mass was defined by the 16 x 16 inch π_3 counter at a distance of 200 inches from the LH_2 target. The p_3 counter (9 x 9 inch) was 500 inches from the target and was overmatched to subtend a somewhat larger solid angle in the center-of-mass. The matched size of the p_3 counter was calculated from the equations

$$\begin{aligned} \Delta H_p &= R_H \, \Delta H_\pi \\ \Delta V_p &= R_V \, \Delta V_\pi \end{aligned} \tag{4}$$

ΔH and ΔV refer to the horizontal and vertical extent of the counters, and F_H and R_V are the horizontal and vertical matching ratios given by

$$R_H = \frac{(L + D)_{eff}^{H,p} \; J_p \sin\theta_\pi}{(L + D)_{eff}^{H,\pi} \; J_\pi \sin\theta_p}$$

$$R_V = \frac{(L + D)_{eff}^{V,p} \; \sin\theta_p}{(L + D)_{eff}^{V,p} \; \sin\theta_\pi} \tag{5}$$

in terms of the effective distances, Jacobians, and laboratory angles. There is a horizontal and vertical focusing effect for both the π and p. Thus in calculating solid angles these effective lengths rather than the measured lengths must be used. They are defined below. L refers to the distance from the H_2 target to the center of the magnet in question, D refers to the distance

from the center of the magnet to the counter in question. Now at 180° scattering we have

$$\frac{\sin \theta_\pi}{\sin \theta_p} = \left(\frac{J_\pi}{J_p}\right)^{1/2} \tag{6}$$

So at 180° the matching ratios become

$$\begin{aligned} R_H &= \frac{(L + D)^{H,p}_{eff}}{(L + D)^{H,\pi}_{eff}} \left(\frac{J_p}{J_\pi}\right)^{1/2} \\ R_V &= \frac{(L + D)^{V,p}_{eff}}{(L + D)^{V,\pi}_{eff}} \left(\frac{J_p}{J_\pi}\right)^{1/2} \end{aligned} \tag{7}$$

ΔH_π and ΔV_π for the π_3 counter were both selected as 16 inches and then ΔH_p and ΔV_p for the P_3 counter were calculated. The effective lengths were calculated using the magnet matrices given by Penner.[9]

The effective lengths are given by

$$\begin{aligned} (L + D)^H_{eff} &= \ell \frac{\cos \beta_2}{\cos \beta_1} + d \frac{\cos \beta_1}{\cos \beta_2} + [\rho + Fd] \sin (\beta_1 + \beta_2) \\ &\quad + F\,[1-\cos(\beta_1 + \beta_2)]\,[\rho + d \tan \beta_2] \end{aligned} \tag{8}$$

$$\begin{aligned} (L + D)^V_{eff} &= \ell + d + (\beta_1 + \beta_2)[\rho - \ell \tan \beta_1 - d \tan \beta_2] \\ &\quad - \frac{\ell d}{\rho} (\tan \beta_1 + \tan \beta_2) \end{aligned}$$

where $\rho = \dfrac{R}{\sin \beta_1 + \sin \beta_2}$

$\ell = L - \frac{R}{2} \sec \beta_1$

$d = D - \frac{R}{2} \sec \beta_2$

R = the effect length of the magnet

β_1 = the incident angle

β_2 = the final angle

L = the distance from the H_2 target to the center of the magnet in question.

D = the distance from the center of the magnet to the counter in question.

and F = is the focusing factor given in general by

$$F \equiv \frac{1}{P}\frac{\partial P}{\partial \theta}$$

and is zero for both π and p for 180° elastic scattering.

Horizontal and vertical effective lengths for both the π and p were calculated using a computer program. The horizontal effective lengths $(L + D)^{H,\pi}_{eff}$ and $(L + D)^{H,p}_{eff}$ differed at maximum from the measured lengths by less than 1%. That is

$$\frac{(L + D)^{H,\pi}}{(L + D)^{H,\pi}_{eff}} = 1.004; \quad \frac{(L + D)^{H,p}_{eff}}{(L + D)^{H,p}} = 1.002 .$$

While for the vertical lengths the maximum ratios were

$$\frac{(L + D)^{V,\pi}}{(L + D)^{V,\pi}_{eff}} = 1.104; \quad \frac{(L + D)^{V,p}}{(L + D)^{V,p}_{eff}} = 1.031$$

So there was more vertical than horizontal focusing.

The center of mass solid angle subtended by the π_3 counter was calculated as follows.

$$(\Delta\Omega)_{CM} = \frac{(\Delta\Omega)_{LAB}}{J_\pi} \qquad (9)$$

where

$$(\Delta\Omega)_{LAB} = \Delta\theta_H^{\pi}\,\Delta\theta_V^{\pi} = \frac{16''}{(L+D)_{eff}^{H,\pi}}\,\frac{16''}{(L+D)_{eff}^{V,\pi}}$$

Typical laboratory solid angles subtended were 7 millisteradians. The solid angle in the center of mass system, defined by the π_3 counter, varied from 1.5 to 0.5 millisteradians as we increased the energy.

The p_3 counter was overmatched to subtend a somewhat larger solid angle in the center of mass than the π_3 counter. The over matching was calculated to allow for such things as the momentum spread and angular divergence of the incident beam, a 1% variation of the magnetic field of the p magnet, a 3% variation of the magnetic field of the π magnet, the H_2 target size, and the multiple Coulomb scattering of the scattered particles.

The horizontal overmatching is given by

$$\delta_H = \left[\left(A\,\frac{\Delta P_0}{P_0}\right)^2 + (B\,\Delta\theta_0)^2 + \left(C\,\frac{\Delta I_p}{I_p}\right)^2 + \left(E\,\frac{\Delta I_\pi}{I_\pi}\right)^2 + (G\,\Delta x_0)^2 + (\sigma_H^*)^2 \right]^{1/2} . \tag{10}$$

The vertical overmatching is given by

$$\delta_V = \left[(B'\Delta\varphi)^2 + (G'\Delta y_0)^2 + (\sigma_V^*)^2 \right]^{1/2} \tag{11}$$

where $A = \alpha_p D_p \dfrac{P_0}{P_p}\dfrac{\partial P_p}{\partial P_0}$

$$B = (L+D)_{eff}^{H,p}\left[1 - \left(\frac{J_p}{J_\pi}\right)^{1/2}\right]$$

$$B' = (L+D)_{eff}^{V,p}\left[1 - \left(\frac{J_p}{J_\pi}\right)^{1/2}\right]$$

$$C = D_p\alpha_p$$

$$E = D_\pi \alpha_\pi R_H \tag{12}$$

$$G = 1 - R_H$$

$$G' = 1 + R_V$$

$$(\sigma_H^*)^2 = \sigma_p^2 + (R_H \sigma_\pi)^2$$

$$(\sigma_V^*)^2 = \sigma_p^2 + (R_V \sigma_\pi)^2$$

The above contribution of the multiple scattering includes both the multiple scattering of the proton and the image of the multiple scattering of the pions. By overmatching the proton counters in this way, in-scattering is equal to out-scattering and no correction to the raw data was necessary.

The various terms making up the overmatching are assumed to be independent of one another and are combined in quadrature. The above overmatching represents about one standard deviation. For most energies we had at least two standard deviations of overmatching.

H. ELECTRONICS AND TIMING

The electronics logic is shown in Figure 9. The three monitor counters ($M_1 M_2 M_3$) formed the M coincidence. The three beam counters (B_1, B_2, B_3) formed the B coincidence which was put in coincidence with the Cherenkov counter forming the $\overline{BC}$ coincidence. The number of $\overline{BC}$ coincidences after corrections yielded the number of pions impinging on our H_2 target. The scattered protons were counted by the p telescope p_1, p_2, p_3 in coincidence. The scattered pions were counted by the π telescope π_2, π_3 in coincidence. The $\overline{BC}$ coincidence and the p coincidence were put in coincidence forming the $p\overline{BC}$ coincidence which formed with the π coincidence the πp fast coincidence and πp slow coincidence.

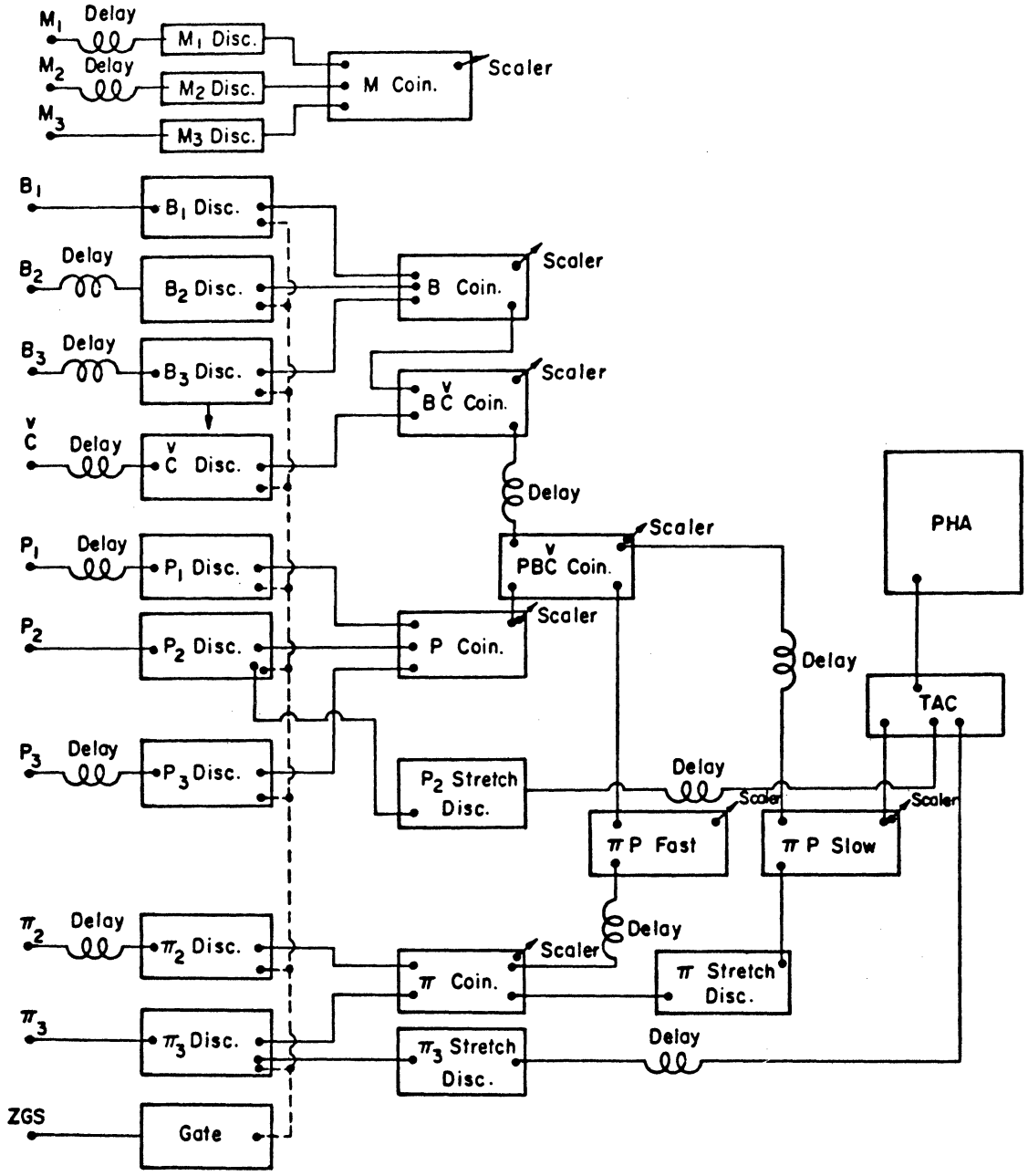

Figure 9. Electronics logic diagram.

The πp fast coincidence had a resolving time of 5 nsec while the πp slow had a resolving time of 30 nsec. These different resolving times were used to check for accidentals.

A pulse height analyzer (PHA) was also used to check for accidentals. Stretched signals from the π_2 and p_2 discriminators were fed directly into a time-to-amplitude converter (TAC) which was gated by the πp slow coincidence. This gave us an output pulse whose voltage was proportional to the overlap time of the π_3 and p_2 pulses. This output was fed into the PHA which gave us a plot of number of events versus the π-p time-of-flight difference. Any significant accidental background would appear as a broad uniform plateau under the elastic peak which could be subtracted from the peak.

We set the pulse height analyzer so that the time difference from one channel to another was approximately 1/3 nsec. We used the first quarter of the memory (100 channels) of the PHA to record the events of a run and the second quarter of the memory to store all the events of a certain energy. The stretched πp coincidence signal which triggered the TAC was 160 nsec long. The p_2 stretched signal was 30 nsec long and the π_3 stretched signal was 50 nsec long. Channel 50 on the PHA corresponded to the normal time of flight difference between the π and p. This gave us a possible range of events of from channel 5 to 95.

All the electronics and the beam magnet controls were housed in an air-conditioned trailer on the ZGS floor. The interior of the trailer with the electronics is shown in Figure 10. This eliminated dirt and noise from the ZGS floor and helped considerably in running the experiment.

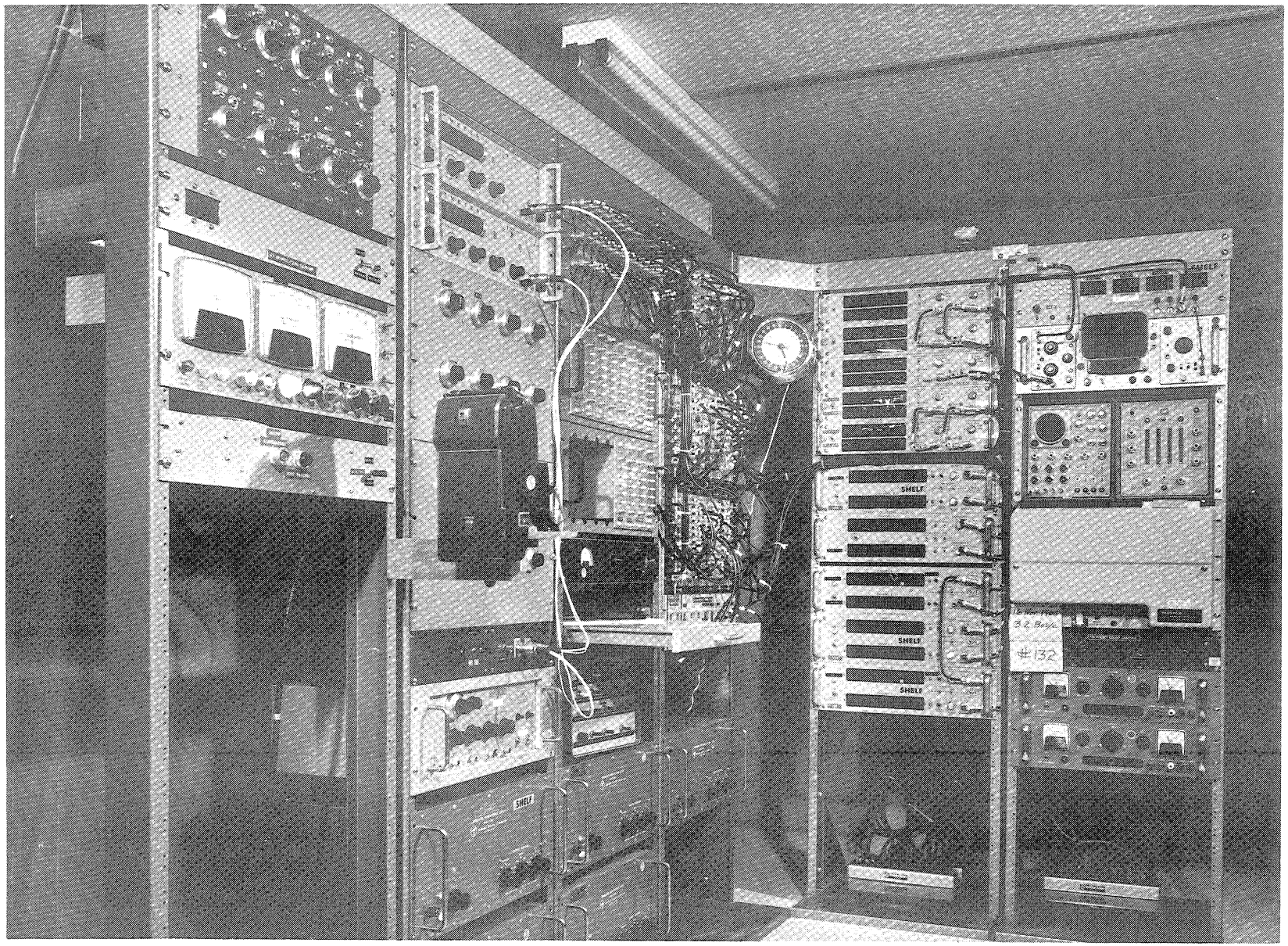

Figure 10. Interior of trailer showing the electronics.

The pulses from the counter phototubes were carried by 50 ohm RG 213 U cables to a trailer panel. Inside the trailer and throughout the electronic logic the signals were carried by 50 ohm RG 223 double shielded cables.

The signal cables from the counters were cut to specified lengths. The pulse transit time was calculated and independently measured for each cable using reflected pulses. The measured pulse transit time of all the signal cables were within one half a nanosecond of the calculated time. The logic cables were made to specified lengths by EG and G.

The timing of the electronics logic circuit including the logic cables and intrinsic discriminator and coincidence circuit delays was first calculated, and then checked by feeding pulser signals into the discriminators and tracing them through the circuits. Thus the approximate delays which we had to insert could be found. These delays were further checked by running a complete set of delay curves at 1.6 GeV/c, our first experimental point, where the counting rate was high. They were all found to be quite close. Delays were then calculated for higher energies.

Typical high voltage curves and delay curves are shown in Figures 11 and 12 respectively. The C counter pressure curve is shown in Figure 13. The dip on the blow up at 84 psig corresponds to 0.6% K's in the beam.

The timing procedure went as follows. First of all the monitor telescope was set up by means of high voltage curves and delay curves on each of the three monitor counters. Then the magnets in the line were set at their calculated values for 1.6 GeV/c momentum, and the beam counters and Cherenkov counter were timed in. For the delay curves, delays were inserted by means of delay boxes

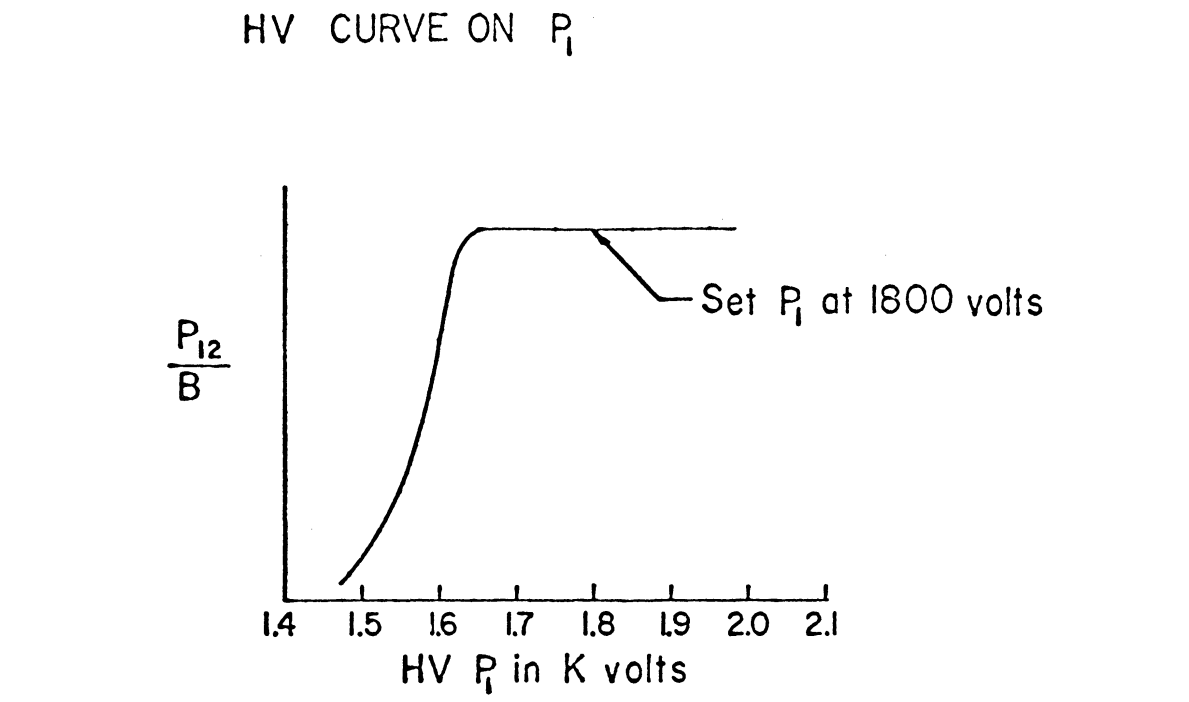

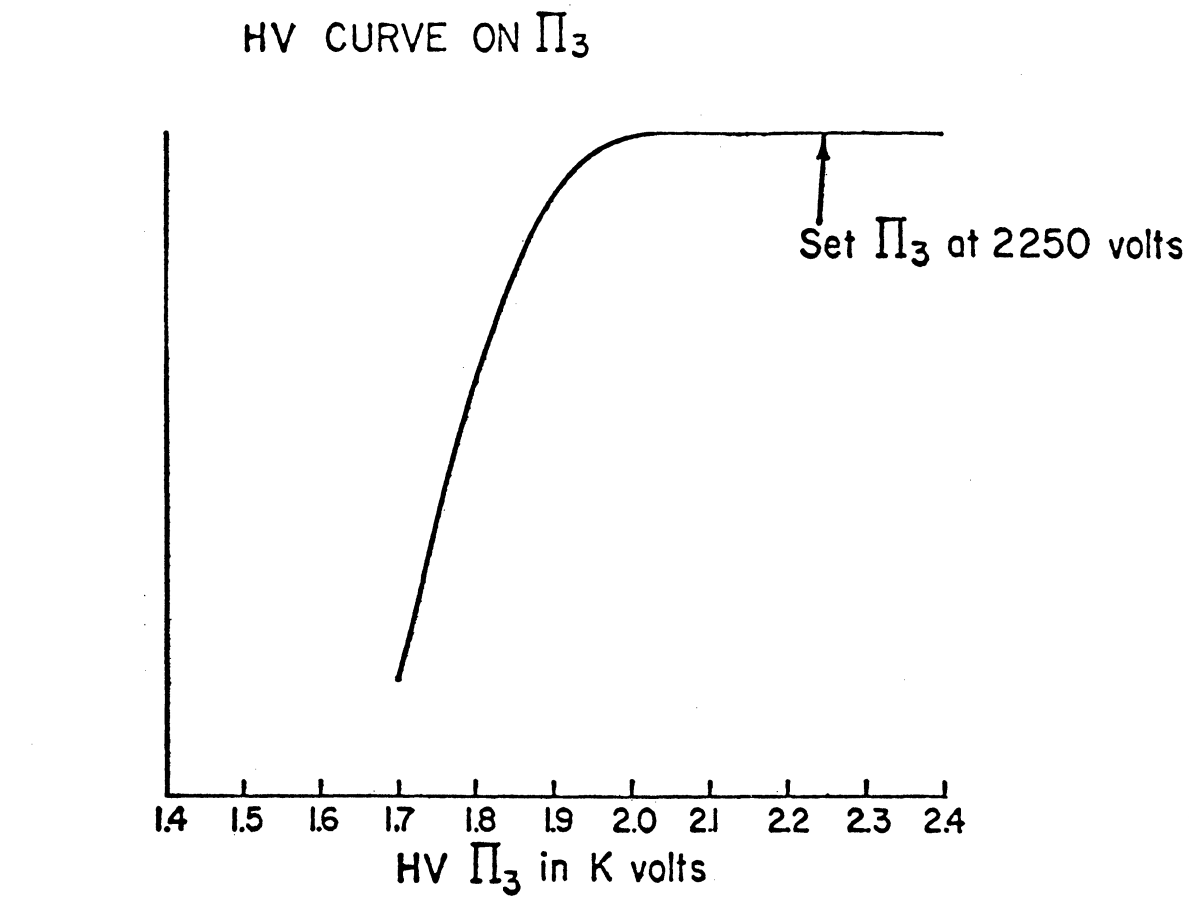

Figure 11. High voltage curves.

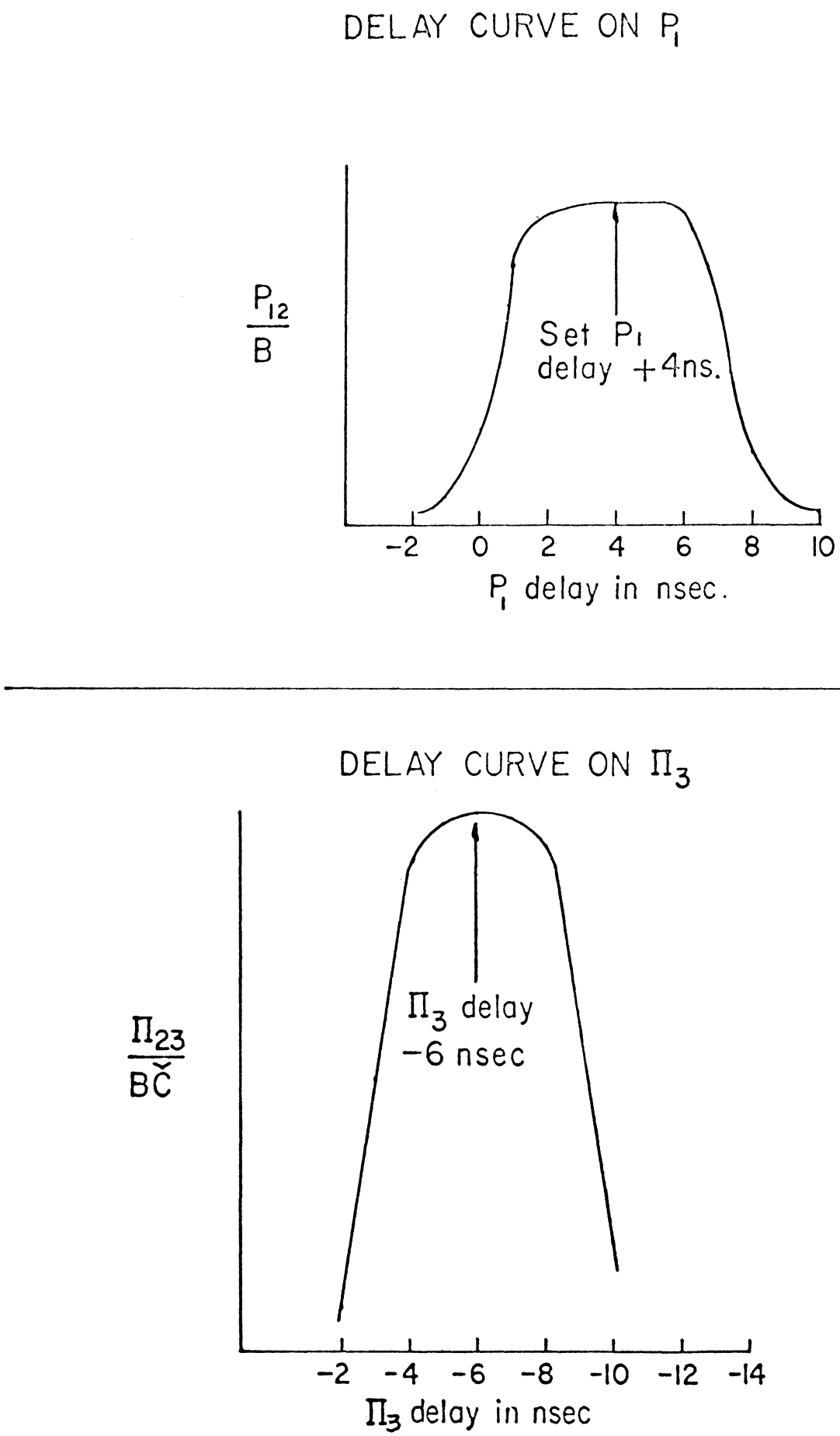

Figure 12. Delay curves.

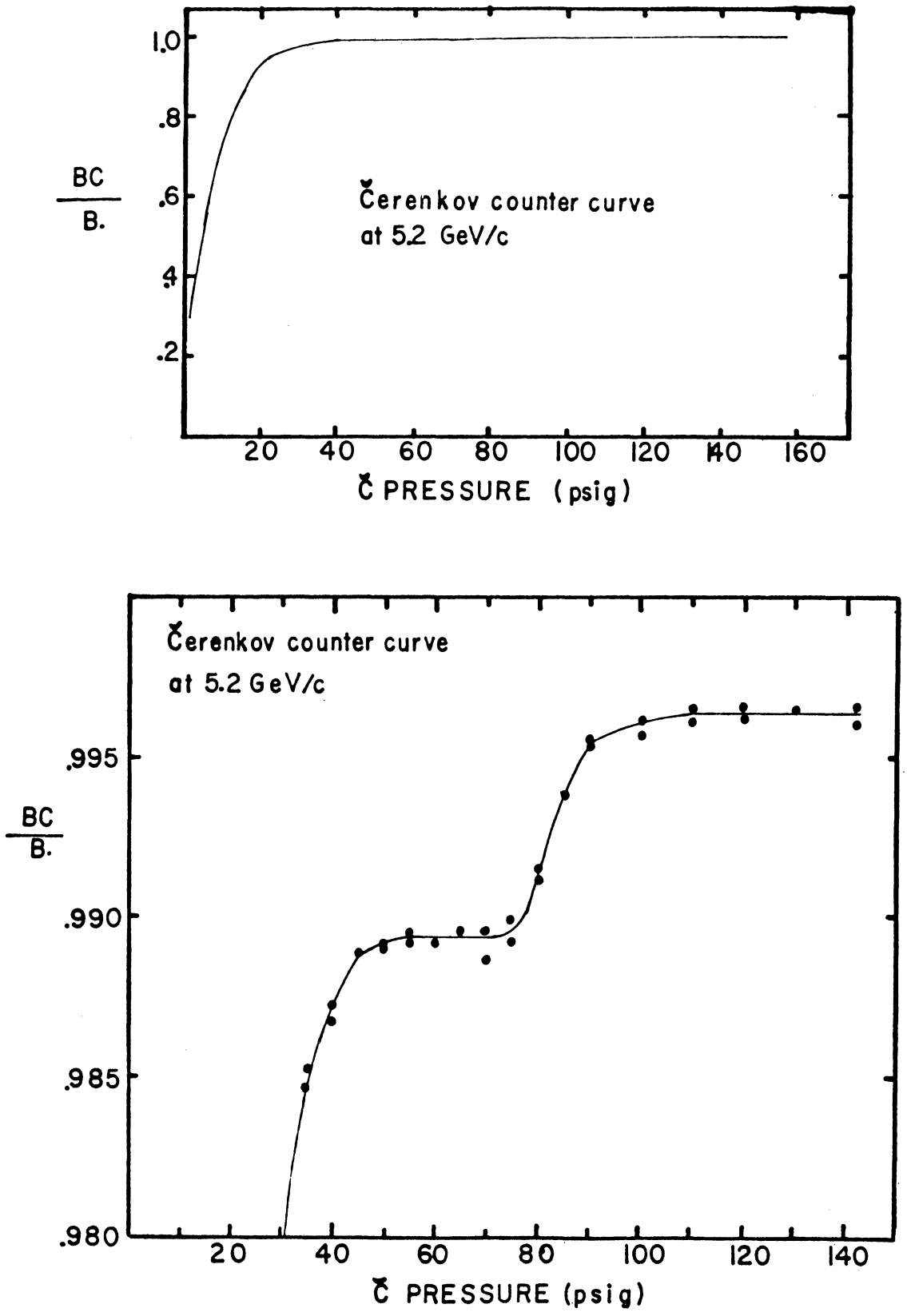

Figure 13. Cherenkov pressure curve.

made by Nanosecond Systems, Inc. The use of these plus the fact that the scalars could be turned off at any preset number by a preset count control made the high voltage and delay curves easy to run. After a delay curve was run and the correct delay determined, a delay cable was inserted in place of the delay boxes. After the beam counters and Cherenkov counter were timed in the beam was tuned for 1.6 GeV/c momentum. After the beam was tuned a Cherenkov counter pressure curve was run. Next the counters in the p and π telescopes were timed in. Then the beam telescope ($B_1B_2B_3\bar{C}$) was timed in with the p telescope. These two telescopes formed the $pB\bar{C}$ coincidence. Then the π telescope was timed in relative to $pB\bar{C}$, to form the final πp fast and slow coincidences.

After we were timed in we ran a p-magnet curve. This consisted in varying the magnetic field of the p magnet around the calculated value and at each point plotting the ratio (πp coincidence)/BC against the p magnet field (Figure 15). It was found that the maximum value of this ratio occurred at the calculated value of the p magnetic field.

Throughout the experiment we could vary the magnetic fields of all our bending magnets and quadrupoles from with our trailer. This was very convenient and timesaving for us. Periodically during the running of the experiment high voltage and delay curves were run on all the counters.

The electronics coincidence system used was a Chronetics Nanologic 100 System. The pulse height analyzer used was a model 404C 400 channel analyzer made by the Technical Measurement Corp. The scalars used were made by Transistor Specialties, Inc. The most important quantities: B, $B\bar{C}$, πp fast and πp slow, were double scaled on two different 100 Mc scalars to insure accuracy. The magnet shunt voltages and the counter high voltages were also monitored by two digital voltmeters in parallel to insure accuracy.

All discriminators except those of the monitors were turned on and off by a gate circuit which was triggered by an Argonne Preset Interval Timer. This timer is synchronized with the ZGS and will give a pulse at any predetermined time after the start of the beam acceleration cycle. The gating times were determined by viewing the gate pulse and the beam spill given by the monitor counters which were simultaneously displayed on a RM 561 A Tektronix oscilloscope. Thus we could bracket the good spill and gate out spikes in the spill.

The run consisted of an integer number of 10^8 BC coincidences. At the end of a run (about 1-2 hours and about 4-6 x 10^8 BC depending on the counter rate) the scalars were automatically turned off at some preset integer number of 10^8 beam particles. We had a Polariod camera (Pathfinder land camera 110A) with a 10 second picture development time permanently mounted with the scalars in focus. At the end of a run we would simply take a picture of the scalars and print out the PHA spectrum. The beam energy, date, run number, and time (from a 24-hour clock) were also recorded on the picture as shown in Figure 14. This method of data recording was straightforward, accurate, and very rapid so we lost little useable beam time.

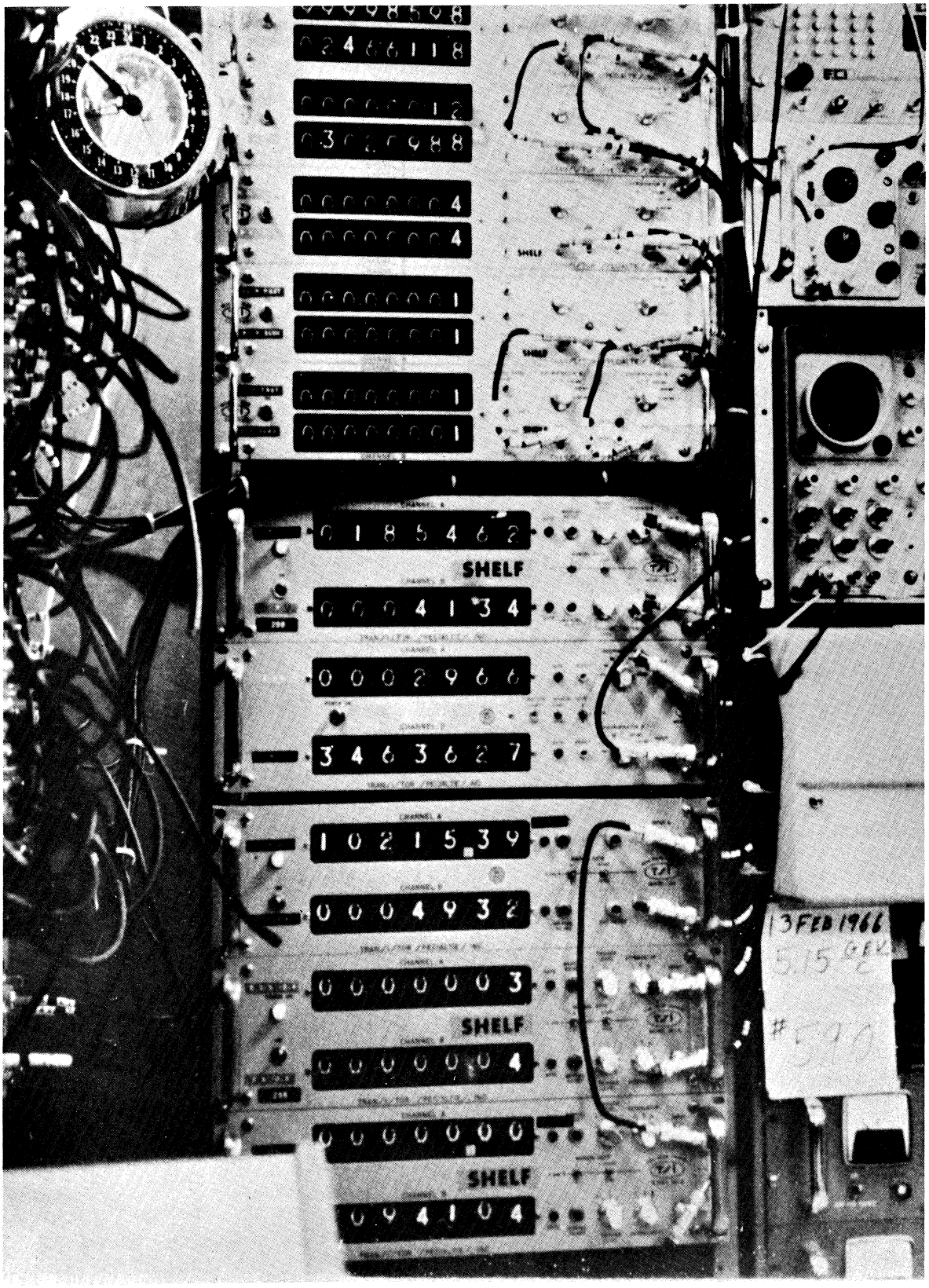

Figure 14. Scalar readings as recorded on Polaroid camera.

III. EXPERIMENTAL CHECKS

At 1.6 GeV/c we ran a p-magnet curve. We purposely detuned the p-magnet and plotted the number of (πp coincidences)/BC versus the magnetic field (see Figure 15). This ratio reached a peak at the calculated value of the magnetic field and decreased on both sides as we went away from the calculated value. This may be regarded as evidence that we were indeed seeing elastic scattering.

We had two methods for studying possible background due to accidental coincidences. The first method involved using two independent πp coincidence circuits; one (πp fast) had a resolving time of 5 nsec and the other (πp slow) had a resolving time of 30 nsec. Both circuits gave essentially the same number of coincidences. This indicated that none of the coincidences were accidental. This was not surprising since the single telescope rates were very low; π was typically 50 counts/pulse and p was about 1 count/pulse.

The alternative method was to feed the signals from the π_3 and p_2 counters directly into a time-to-amplitude converter (TAC). This gave out a pulse whose amplitude in volts was proportional to the overlap time of the π_3 and p_2 pulses. This output was fed into a TMC 400-channel pulse-height analyzer (PHA), which gave us a plot of number of events against the π-p time-of-flight difference. The peak was typically about 3 nsec wide (see Figure 16). Two nsec of this was due to the fact that the H_2 target was 12" long. The additional time spread was caused by small time differences in light transit time in the scintillators and light pipes, small time differences in the photomultiplier tube responses, and small time differences in the various logic circuits.

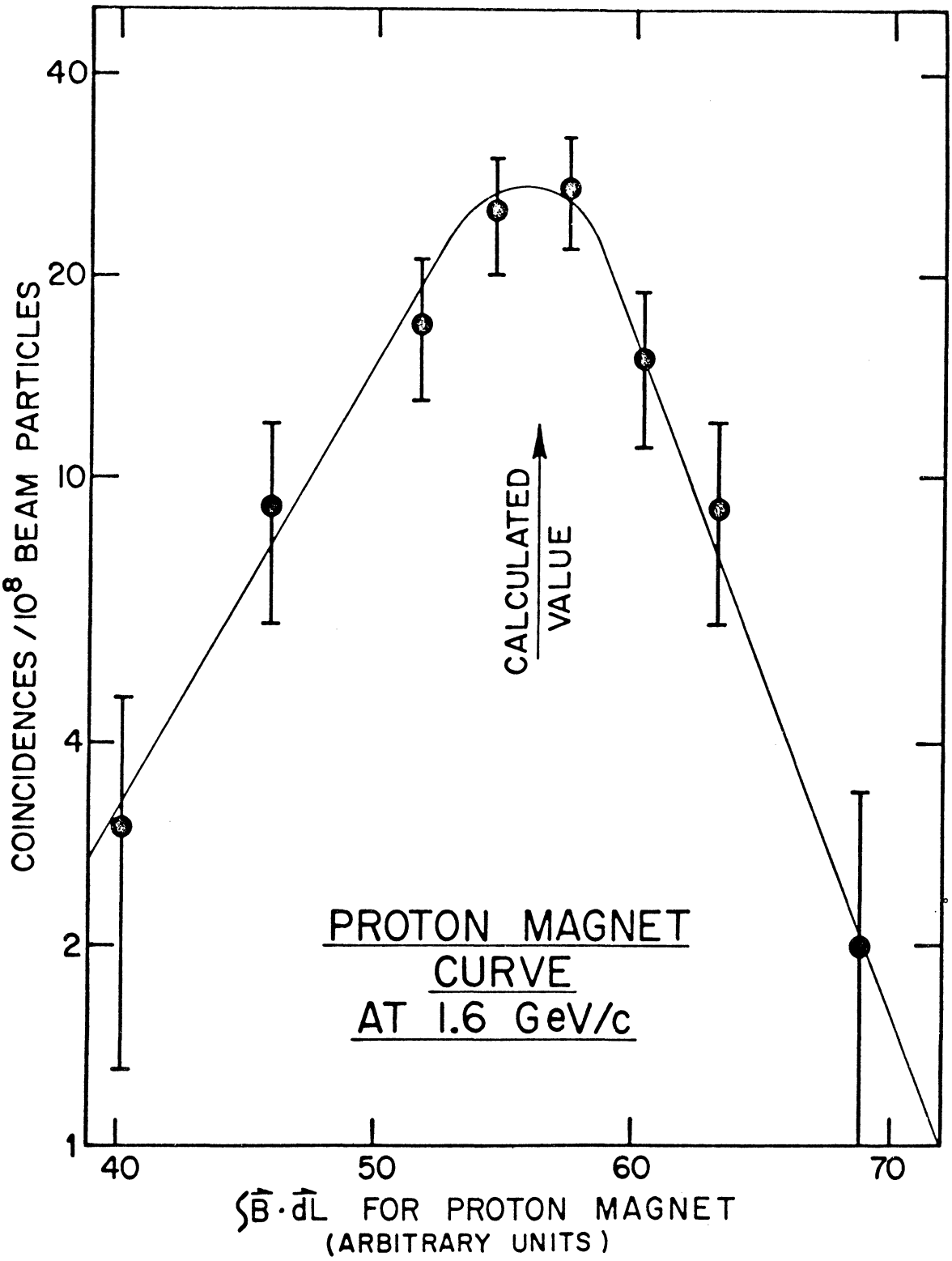

Figure 15. Proton magnet curve.

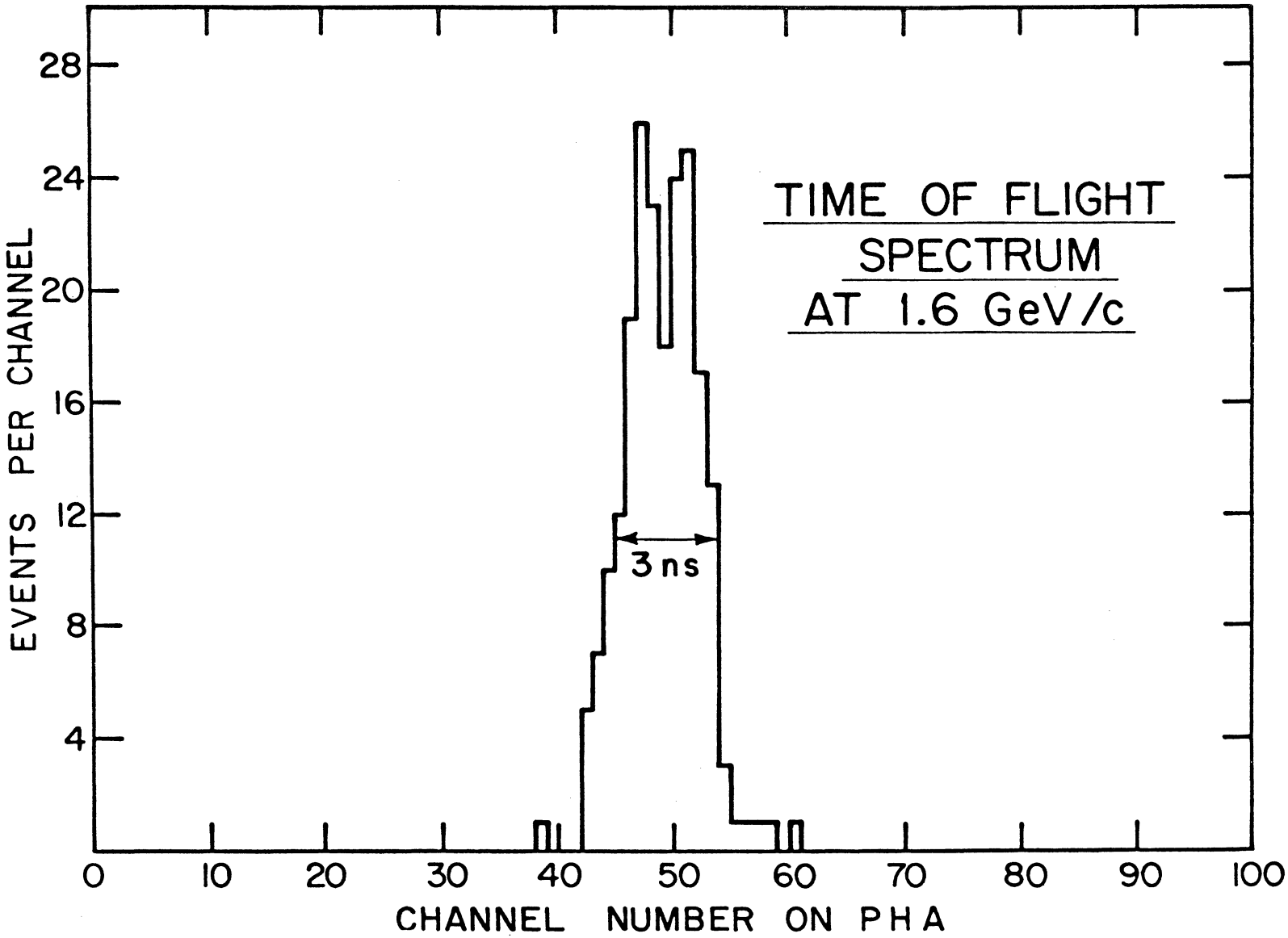

Figure 16. Pulse height analyzer time of flight spectrum.

Any significant accidental background would have shown itself as a broad plateau under the elastic peak which could be subtracted from the peak. The events which were outside of approximately a 15 channel range ($\approx$ 5 nsec) about the peak we regarded as accidental and disregarded in our cross section calculation. There were only a small number of these, typically 1 or 2 per hundred events.

We wanted to show that there was no contamination due to inelastic events of the type

$$\pi^- + p \rightarrow \pi^- + p + \pi^\circ \quad . \tag{13}$$

This was done by taking data runs with a 2-1/2" long carbon target placed just behind the empty LH_2 target. This carbon target had about three times the number of protons as the LH_2 target but the protons in the carbon nucleus had some Fermi momentum. The Fermi momentum is distributed isotropically and has a range of up to a maximum of about 0.230 GeV/c.

Suppose our constraints on angle and momentum were sufficiently lax that with the LH_2 target we were observing π^-p events that were in fact smeared by π° production. Then the additional smearing of angle and momentum introduced by the Fermi momentum of the protons in the carbon nucleus would not remove the counting rate. But if our kinematic constraints were sufficiently tight that the smear of the Fermi momentum removed most of our event rate, then we have evidence that π° production smears things too much to be detected much by our double spectrometer. This is true because the π° production introduces a greater smear than the Fermi momentum for any reasonable distribution of π° mesons. We took several runs with a carbon target at different energies and

obtained two events. In equivalent runs with a H_2 target we obtained over a hundred events. This conclusive evidence for a 1% upper limit on inelastic contamination. It also showed that we had no accidental events. This is seen as follows. With the carbon target in place of the LH_2 target the number of coincidences in the π telescope remained the same but the number of PBC coincidences increased. The ratio of $\overset{v}{PBC}_{carbon}/\overset{v}{PBC}_{LH_2}$ was 2 at 2.8 GeV/c and 1.5 at 4.1 GeV/c. Therefore, if we were counting accidental events we should have seen more with the carbon target. However, we saw only two events compared to over a hundred with the LH_2 target. Thus we conclude that we had no accidental events. The carbon runs simultaneously served as empty-target runs as the carbon target was placed just behind the empty LH_2 target.

IV. CORRECTIONS AND UNCERTAINTIES

This section describes the corrections and uncertainties which were applied to the data.

A. NUCLEAR INTERACTIONS

Some of the desired events were not recorded because the pion and/or proton did not travel completely through their respective telescopes because of nuclear interaction in the hydrogen target, air, or scintillators. The number of events lost in this manner can be calculated if the relevant cross sections are known. A good approximation to the actual cross section is the natural or geometrical cross section defined by $\sigma_{natural} = \pi r_n^2$ where $r_n = (\hbar/m_\pi c)A^{1/3}$ is the nuclear radius, $\hbar/m_\pi c = 1.4$ Fermi, and A the mass number of the material. We can improve this formula by remembering that in the energy region we are dealing with a nuclear collision can be thought of as occurring between the incoming particle and the individual nucleons of the nucleus. p-p and π-p collision cross sections are experimentally known. So the collision cross section for other materials can be better approximated by multiplying the natural cross section by the ratio of the p-p (or π-p) experimental cross section to the natural cross section for A = 1. Thus we have

$$\begin{aligned} \bar{\sigma}_{pA} &= \bar{\sigma}_{pp} A^{2/3} \\ \bar{\sigma}_{\pi A} &= \bar{\sigma}_{\pi p} A^{2/3} \end{aligned} \qquad (14)$$

where $\bar{\sigma}_{pp}$ and $\bar{\sigma}_{\pi p}$ are the average proton-proton and pion-proton total cross sections in our energy range and are taken to be 45 and 30 mb respectively.[10-11]

Some of the interacting particles yield forward going charged particles that are still counted. We estimate that of those interacting in the hydrogen target 20% ± 10% are still counted; of those interacting in the air 30% ± 10% are still counted; of those interacting in the scintillators 50% ± 15% are still counted. So we have for the proton correction

$$\exp\left\{\bar{\sigma}_{pp} N_0 \left[\left(\frac{\rho L_p}{A^{1/3}}\right)_{AIR}(.70\pm.10) + \left(\frac{\rho L_p}{A^{1/3}}\right)_{SCIN}(.50\pm.15) + \left(\frac{\rho t/2}{A^{1/3}}\right)_{LH_2}(.80\pm.10)\right]\right\} \qquad (15)$$

where N_0 = Avagadro's number = 6.023×10^{23}

ρ = density of the various materials in g/cm^3

L_p = path length of proton in the various materials

t = H_2 target length = 30.5 cm.

There is a similar expression for the pion correction. Combining these two expressions we have a total nuclear interaction correction of (12.5 ± 2.5)%.

B. DECAY OF PIONS

The pion is unstable decaying into a muon and a neutrino with a mean life of 25.5 nsec[12] in its rest frame. As many as 30% of the backward scattered pions decayed before reaching the final counter in the pion telescope. However, the muons were emitted by the relativisitic backward scattered pions in a narrow forward cone with a maximum half angle of from 6.4 degrees at 1.6 GeV/c incident beam energy to 5.4 degrees at 5.3 GeV/c. The backward scat-

tered pion momentum varies slowly over the energy range of the experiment. At an incident beam energy of 1.6 GeV/c the momentum of the scattered pion is 0.352 GeV/c; at 5.3 GeV/c it is 0.420 GeV/c. Thus the coincidence was completed in many cases by the muons. Also events lost by the muon missing the pion counters were somewhat compensated for by pions which would have missed the counters being counted by decaying and sending a muon through the counter.

We assume that all those back scattered pions which decay in the first 80 inches before the π-magnet are lost that is their muon does not go through the pion counter telescope. We also assume that the pions which decay in the remainder of the path are counted via their muon or by a compensating muon coming into the telescope. Since the momentum of the scattered pions does not vary much, this correction is practically energy independent. With these assumptions the correction for the decay of the scattered pions is $(9\pm5)\%$.

Admittedly this is a somewhat rough calculation. To do it more accurately would require a complicated Monte Carlo program and still one could not properly fold the beam divergence and momentum spread into the program. Since the correction is small anyway, the above calculation is sufficient.

Some of the incident beam pions decay from B_3 to the liquid hydrogen target. However, this distance is only a few inches so this correction was well below 1%.

C. MUON CONTAMINATION

To get a rough idea of the magnitude of the muon contamination we did the following experiment. We inserted 30 inches of brass (about 6 collision lengths using the geometrical cross section) into the beam and measured the beam with

and without the brass in the beam. Since pions interact strongly they should be removed by the brass while the muons which interact electromagnetically for the most part pass through the brass. We did this measurement at three different energies and from the ratios of the scalars got for muon contamination the values 6.8% at 5.2 GeV/c, 6.1% at 3.6 GeV/c, and 4.9% at 2.6 GeV/c.

This measurement is rather difficult to do accurately. There will be multiple Coulomb scattering effects of the muons depending on their laboratory angular distribution. Some of the pions which undergo strong interactions will be forward scattered and counted as muons. At higher energies less pions decay but they are restricted to a smaller forward cone. At lower energies more pions decay, but their forward cone is larger. These effects work against each other but it is difficult to accurately calculate them.

As a final correction we decided on a muon contamination of $(6 \pm 2)\%$ for all energies.

D. ELECTRON CONTAMINATION

Since the range of electrons in copper is 7 to 9 cm in an energy range of 1.6 to 6.0 GeV/c clearly the electrons in the beam, if any would be stopped by the 30 inches of brass which we inserted into the beam to measure the muon contamination.

We measured the electron contamination in the beam by running a $\check{C}$ pressure curve down to zero psig of ethane and established that there was less than 1% electron contamination in the beam.

E. COUNTING LOSSES IN BEAM COUNTERS

More beam particles than we count hit the H_2 target while the coincidence circuitry is activated. The pulse width of all our logic electronics was 2.5 nsec. If, during this time, 2 or more beam pions pass through our beam counters only one will be counted yet all of them hit our H_2 target, can interact to produce an event, and be counted by the activated coincidence electronics as an event.

We are not concerned about beam pions which pass through the beam counters during any dead time of the beam counters or the beam logic circuits. Since the beam telescope is in coincidence with both the π and p telescopes, we must get a beam coincidence in order to get an event. So those beam particles which arrive at any portion of the beam circuit dead time except during the 2.5 nsec while the coincidence circuitry is activated are completely excluded from the cross section measurement and we need not concern ourselves with them.

The probability of two particles separated in time by less than 2.5 nsec both interacting to give events is extremely small. Therefore to a very high degree of accuracy only the number of beam particles impinging on the LH_2 target should be modified.

The counting loss can be written as

$$\text{loss} = 1P_2 + 2P_3 + 3P_4 + \ldots$$

Consider for example the second term on the right side in the above expression. P_3 is the probability of 3 beam pions in the time T, the pulse width of our electronics, given one event. The coefficient 2 arises because we count the first pion but miss the next two. So

$$P_2 = \frac{\text{absolute probability of 2 events in time T}}{\text{absolute probability of 1 event in time T}} \tag{16}$$

Using Poisson statistics we have

$$P_2 = \frac{(m^2/2!)\ e^{-m}}{(m/1!)\ e^{-m}} = \frac{m}{2!}\ ;\ m = aT \tag{17}$$

where a is the average counting rate and T is the time interval under consideration. Also

$$P_3 = \frac{m^2}{3!} \tag{18}$$

and so on. Using the above the loss becomes

$$\text{loss} = \frac{m}{2} + \frac{m^2}{3} + \frac{m^3}{8} \cdots \tag{19}$$

While the protons are accelerated they form RF bunches 8 nsec long every 80 nsec. During the spill the beam still has this approximate structure, therefore the effective spill time will be 1/10 of the measured spill time. Assuming no ZGS magnet ripple, a measured spill of 150 nsec, and a beam intensity of 2.0×10^5 pions per pulse we get a beam counting loss of $(2 \pm 1)\%$. The measured denominator $(\bar{BC})$ is too small by approximately $(2 \pm 1)\%$. It should be increased by $(2 \pm 1)\%$. Therefore the cross section should be decreased by approximately $(2 \pm 1)\%$.

F. EVENTS OCCURRING IN THE BEAM COUNTERS

A $(2 \pm 1)\%$ subtraction was made for interactions occurring with the hydrogen of the polystyrene of the B_2 and B_3 beam counters. Our system detected these interactions. In fact these events can be seen as high channel events on the PHA time of flight spectrum (Figure 16). Their high

channel number and thus their relative time of flight difference (pion early, proton late) as well as their relative number correspond to expected events from these two beam counters.

G. INELASTIC CONTAMINATION

As was mentioned earlier we measured the inelastic contamination to have an upper limit of 1%.

H. BIN SIZE

In a counter experiment it is impossible to measure the differential cross section at exactly a given point because of the finite size of the counters. Thus in this experiment we measured the average cross section within an angular spread $\Delta\theta$ around 180°. Our CM subtended angle $\Delta\theta$ varied from 1° to 0.4° as we increased the energy. Although there is structure in the differential cross section as a function of angle close to 180° it is not sufficiently violent to change much over this range.

I. COUNTER EFFICIENCY

Early tests of the counters with both cosmic rays and with the π^- beam showed them to to be essentially 100% efficient. High voltage and delay curves were run periodically on all the counters in the system. Throughout the experiment we assumed the counters to be 100% efficient and thus have no correction for counter efficiency.

As was mentioned earlier we ran periodic high voltage and delay curves on the counters to check the timing and efficiency.

J. BEAM ATTENUATION IN LH_2 TARGET

As the incident pion beam moves through the target, pions are removed by interaction with the target protons so that fewer pions are available to interact at the downstream end of the target than at the upstream end. This effect is an overall reduction in the effective beam intensity. The effective beam intensity, I_{eff}, is given in terms of the incident beam intensity I_o by

$$I_{eff}t = \int_0^t I(x)dx \quad \text{or}$$
$$I_{eff} = \frac{I_o}{t}\int_0^t e^{-\bar{\sigma}_{\pi p}\rho x}\,dx \tag{20}$$

where t is the target length, $\bar{\sigma}_{\pi p}$ is the average $\pi^- p$ total cross section in our energy range and ρ is the number of protons per cubic centimeter in the liquid hydrogen target. The x-axis points along the beam direction with its origin at the upstream edge of the target. The resulting expression of I_{eff} is

$$I_{eff} = I_o\left(1 - \frac{\bar{\sigma}_{\pi p}\rho t}{2}\right) \tag{21}$$

Taking $\bar{\sigma}_{\pi p}$ = 30mb in our energy range and assuming that all pions which interact once are lost to the beam, we get

$$I_{eff} = 0.99\ I_o\ .$$

K. UNCERTAINTY IN THE PION JACOBIAN

The solid angle in the center of mass subtended by the defining pion counter is given by:

$$(\Delta\Omega)_{CM} = \frac{(\Delta\Omega)^{\pi}_{LAB}}{J_\pi}\ . \tag{22}$$

At 180°

$$J_\pi = \frac{1 - \beta_{CM}^2}{(g_\pi - 1)^2} \tag{23}$$

where

$$\beta_{CM} = \frac{P_{inc}}{E_\pi + m_p} \quad ; \quad g_\pi = \frac{m_\pi^2 + m_p E^\pi_{inc}}{m_p^2 + m_p E^\pi_{inc}} \tag{24}$$

$$E^\pi_{inc} = (P^2_{inc} + m^2_\pi)^{1/2}$$

Because of the uncertainty in the pion beam momentum P_{inc} of $\pm$ 0.03 GeV/c there is an uncertainty in J_π. This uncertainty varies from $\pm$ 1.5% at 1.60 GeV/c to $\pm$0.5% at 5.3 GeV/c.

V. RESULTS AND CONCLUSIONS

The differential cross section in the center-of-mass was calculated from the formula

$$\left(\frac{d\sigma}{d\Omega}\right)_{CM} = \frac{(\pi p\overset{\vee}{BC})/\overset{\vee}{BC}}{\frac{N_o pt}{A}\frac{\Delta\Omega}{J_\pi}} \quad (abcdefgh) \qquad \text{where} \tag{25}$$

where $(\pi p\overset{\vee}{BC})$ = total number of elastic events at a given energy

$(\overset{\vee}{BC})$ = number of beam coincidences at a given energy

N_o = Avagadro's number = 6.023×10^{23}

ρ = density of liquid hydrogen = .071 g/cc

t = length of the H_2 target = 30.5 cm

$\Delta\Omega$ = solid angle subtended by the π_3 counter in the laboratory

J_π = the pion Jacobian

A = atomic weight of hydrogen = 1.01

a = correction for nuclear interaction = $1.12 \pm .02$

b = correction for decay for π = $1.09 \pm .05$

c = correction for muon and electron contamination in beam = $1.06 \pm .02$

d = correction for counting losses in beam counters = $.98 \pm .01$

e = correction for events occurring in B_2 and B_3 beam counters = $.98 \pm .01$

f = correction for inelastic contamination = $.99 \pm .01$

g = correction for beam attenuation in LH_2 target = 1.01

h = correction for uncertainty in the pion Jacobian = $1.00 \pm .01$.

Combining all the corrections and errors we get a net correction to the

raw data of 1.25 with a maximum error of ± 12%. That is (abcdefgh) = (1.25 ± .12).

The above systematic error appears primarily as a normalization uncertainty. As was previously discussed we used essentially the same layout in measuring the cross section at adjacent energies. In view of this there should be no relative systematic errors. However, in addition to the 12% normalization uncertainty, there may very well be an energy dependant uncertainty of 3% in going from 1.6 to 5.3 GeV/c.

The statistical errors which represent one standard deviation are for the most part in the range of 10% to 15%. The uncertainty in the beam momentum is ± 0.03 GeV/c. The angle subtended by our counters around 180° varied from 1° to 0.4° as we increased the energy.

The cross section for π^-p elastic scattering at 180° as a function of laboratory pion momentum is given in Table II and is shown graphically in Figure 17. Only the statistical errors corresponding to one standard deviation are shown. The line is a freehand fit to the data. The positions of the known N* resonances are shown. Given below them are their masses in MeV and their quantum numbers: isotopic spin, spin, and parity. Other groups have measured the π^-p elastic scattering cross section at angles between 160 and 180° in the center of mass[1-7] although they did not get back as far as 180°. Our data agrees fairly well with them.

In elastic scattering each resonance appears as an intermediate state in the process

$$\pi^- + p \rightarrow N^* \rightarrow \pi^- + p.$$

TABLE II

CENTER OF MASS CROSS SECTIONS FOR
π^-p ELASTIC SCATTERING AT 180°

P_0[a] (GeV/c)	S $(GeV)^2$	$d\sigma/d\Omega$ (μ^b/sr)	$d\sigma/dt$ $\mu^b/(GeV/c)^2$	Error[b] (%)
1.60	3.91	220	1200	7
1.70	4.10	127	643	10
1.80	4.29	89.8	424	10
2.00	4.66	15.5	64.5	12
2.10	4.85	3.15	12.4	23
2.20	5.04	3.29	12.2	23
2.30	5.22	8.04	28.3	18
2.40	5.41	21.6	72.4	11
2.50	5.60	33.3	106	9
2.60	5.79	31.9	97.4	10
2.65	5.89	36.9	110	11
2.70	5.98	41.3	121	10
2.80	6.16	42.1	118	11
2.90	6.35	40.1	108	11
2.95	6.45	27.5	72.7	12
3.00	6.54	20.8	53.9	11
3.10	6.73	23.7	59.2	10
3.15	6.82	20.1	49.3	12
3.20	6.91	15.9	38.3	11
3.30	7.10	14.5	33.7	12
3.40	7.29	13.5	30.4	12
3.50	7.48	13.0	28.3	9
3.55	7.57	12.6	27.0	15
3.60	7.66	16.9	35.6	10
3.70	7.85	14.2	29.1	11
3.80	8.04	14.0	27.8	12
3.90	8.23	16.9	32.6	12
3.95	8.32	16.6	31.6	12
4.00	8.41	16.0	30.0	12
4.10	8.60	13.2	24.1	12
4.20	8.79	11.9	21.1	13
4.30	8.98	10.1	17.5	14
4.40	9.16	9.44	15.9	15
4.50	9.35	9.60	15.8	16
4.60	9.54	10.7	17.2	15
4.65	9.63	7.58	12.0	12
4.70	9.73	9.50	14.9	15
4.80	9.91	6.77	10.4	15
4.90	10.10	7.07	10.6	17
5.00	10.29	6.38	9.37	18
5.05	10.39	8.21	11.9	19
5.10	10.48	10.7	15.4	15
5.15	10.57	10.4	14.8	17
5.20	10.66	7.25	10.2	22
5.30	10.85	6.73	9.28	20

[a]The laboratory momentum P_o is known to $\pm$ 0.03 GeV/c.

[b]The errors quoted are statistical corresponding to one standard deviation. There is also a maximum normalization error of $\pm$ 12%.

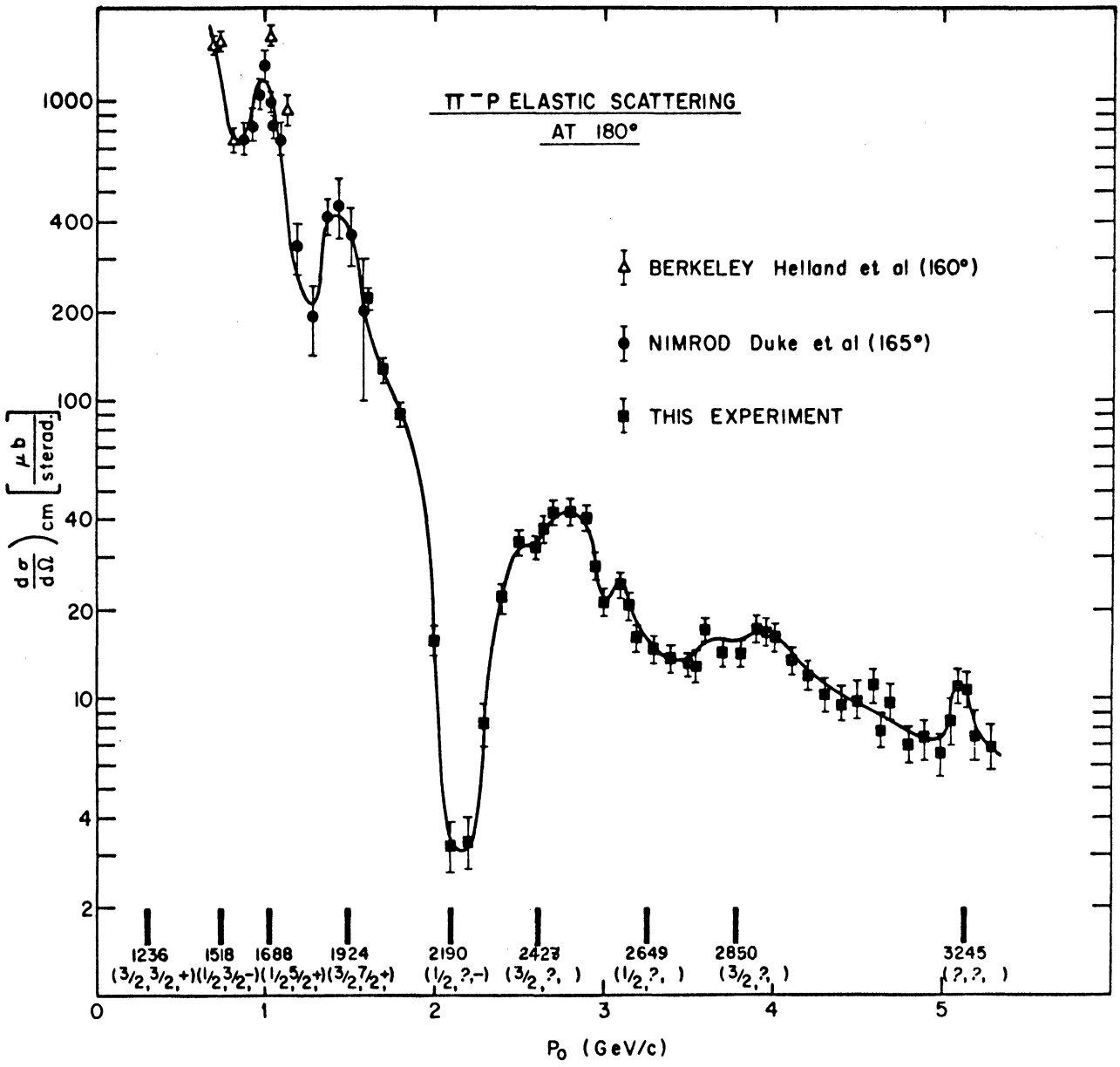

Figure 17. The center of mass cross section for π^-p elastic scattering at 180° as a function of laboratory pion momentum. The cross section is in μb/sterad. The pion momentum in GeV/c. Only the statistical errors corresponding to one standard deviation are shown. The line is a freehand fit to the data. The positions of the known N* resonances are shown. Given below them are their masses in Mev and their quantum numbers; isotopic spin, spin, and parity.

In this type of process there are effects due to two types of amplitudes, the resonance amplitude and the non-resonant elastic amplitude or background amplitude. These two amplitudes may interfere constructively or destructively or not at all. There is a dramatic destructive interference at P_o = 2.15 Gev/c which is quite interesting as the cross section drops almost two orders of magnitude in this region.

Another interesting result of the experiment is the large narrow peak in the cross section at P_o = 5.12 GeV/c. We believe that this is firm evidence for the existence of a nucleon resonance with a mass of 3245 $\pm$ 10 Mev. This N* (3245) has a full width at half-maximum of less than 35 Mev and rises about 4μb/sterad above the non-resonant cross section. The width of the resonance is about 1% of its mass. This means that the particle is quite long lived in spite of its large mass.

The parities and the quantity X(J + 1/2) of the N* resonances were calculated as follows. Using the idea first suggested by Ross and Heinz, at 180° the elastic $\pi^- p$ differential cross section in the region of a resonance can be written as[13,14,22]

$$\frac{d\sigma}{d\Omega} = \left| A_B^{NF} + \frac{\lambda C X(J + 1/2)\ (-1)^{\ell}}{\epsilon - i} \right|^2 \qquad (27)$$

since at 180° the spin-flip terms are zero. In equation (27) C is the Clebsch-Gordan coefficient

$$C = 1/3 \text{ for } I = 3/2$$

$$C = 2/3 \text{ for } I = 1/2$$

X = the elasticity of the resonance Γ^e/Γ

Γ = the full width at half maximum of the resonance

Γ^e = the partial width for decay into the elastic channel

J = the spin of the resonance

$\epsilon = M_R^2 - S/M_R\Gamma_R$

M = the mass of the resonance

S = the square of the center of mass energy

A_B^{NF} = the non-spin-flip background amplitude

We can write $(-1)^\ell$ in terms of the parity of the resonance, P_R. the π^-p system $P_{\pi^-p} = (-1)(+1)(-1)^\ell$ and since the resonance formation and decay are parity conserving reactions

$$P_R = P_{\pi^-p} = -(-1)^\ell . \tag{28}$$

So we can write the resonance amplitude R as

$$R = -\frac{\lambda CX(J + 1/2)\ P_R}{\epsilon - i} \tag{29}$$

If the partial widths of the various channels have the same energy dependence (usually a good approximation in the energy region $E_R \pm 3/2\ \Gamma_R$) the above resonance amplitudes trace out circles in the complex plane.[15] The diameter of the circle is equal to the magnitude of the pure imaginary part of the resonance amplitude when $\epsilon = 0$, that is at the resonance energy. The circle is above or below the real axis depending on the parity of the resonance. See Figure 18. Starting at an energy below a resonance and increasing the energy, the circles are traversed in a counterclockwise direction starting at the

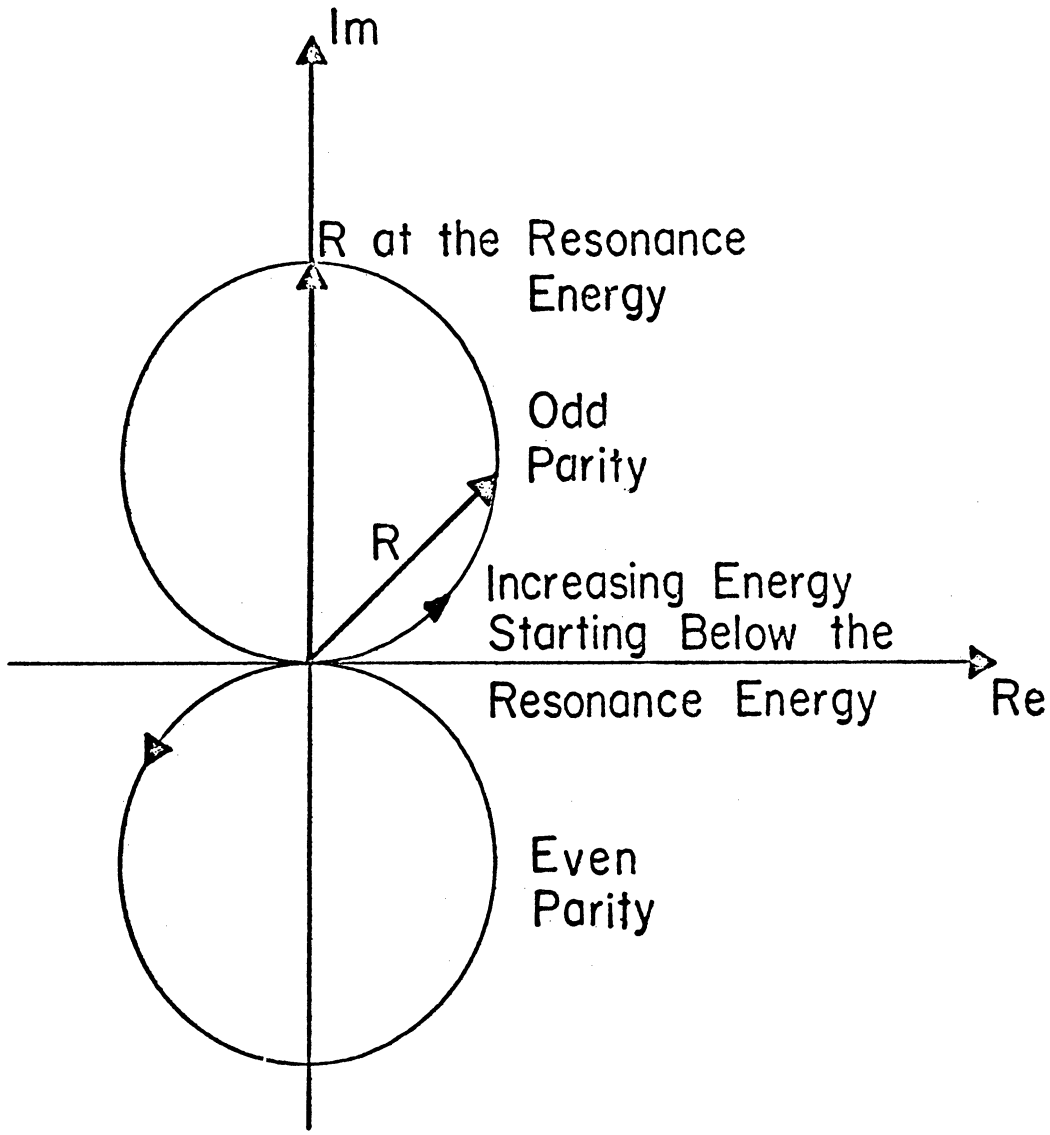

Figure 18. Resonance amplitude in the complex plane.

origin. At the resonance energy, R is a maximum, is pure imaginary, and is at the top, or bottom, of the circle depending on the parity of the resonance.

If there is also a non-resonant background amplitude present, the circular trajectory is still traced out but the starting point is displaced from the origin and the resonance energy is no longer at the top, or bottom, of the circle. That is the maximum intereference, constructive or destructive, does not occur at the resonance energy but is displaced from it. See Figures 19 and 20.

For the background cross section we used the empirical form

$$\frac{d\sigma}{d\Omega} = A(P^{\pi^-}_{LAB})^a \ \mu b/sr \qquad (30)$$

where

$P^{\pi^-}_{LAB}$ = is the momentum of the incident π^- in the laboratory

A = 420

a = -2.58

This was obtained from a straight line fit to the data on a log-log plot. The assumed background cross section is shown as a dashed line in Figure 21.

It is assumed that the sign of the real and imaginary parts of the background amplitude do not change sign as a function of energy. We can determine the quadrant of the background amplitude as follows. The N* (1688) and the N* (1924) both interefere constructively with it near their resonant energies. They are known[16] to have positive (+) parity. From this we assume that the background amplitude does not lie in the first or second quadrant because if it did it would not interefere constructively with the positive parity reso-

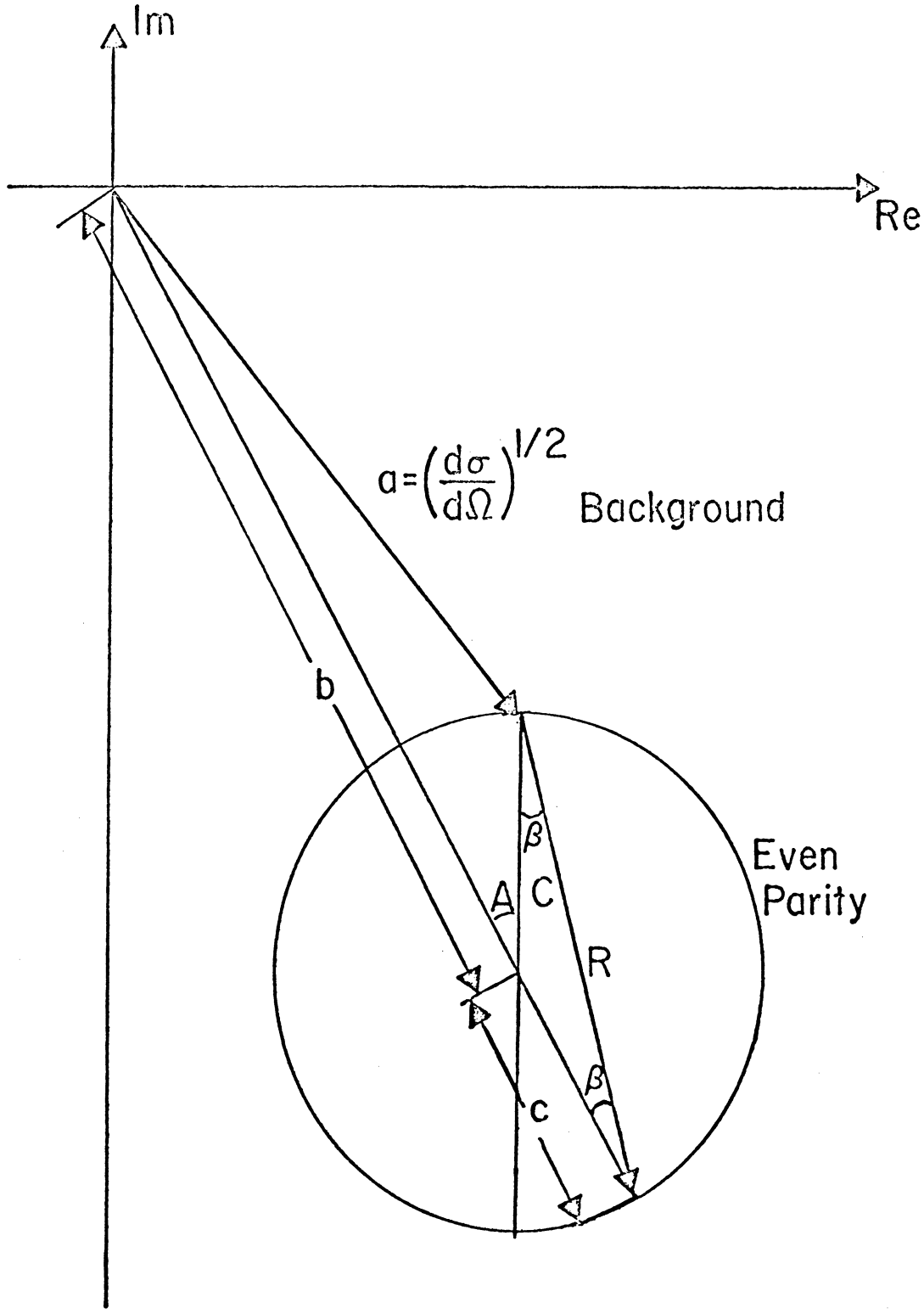

Figure 19. Constructive interference of background and resonance amplitudes.

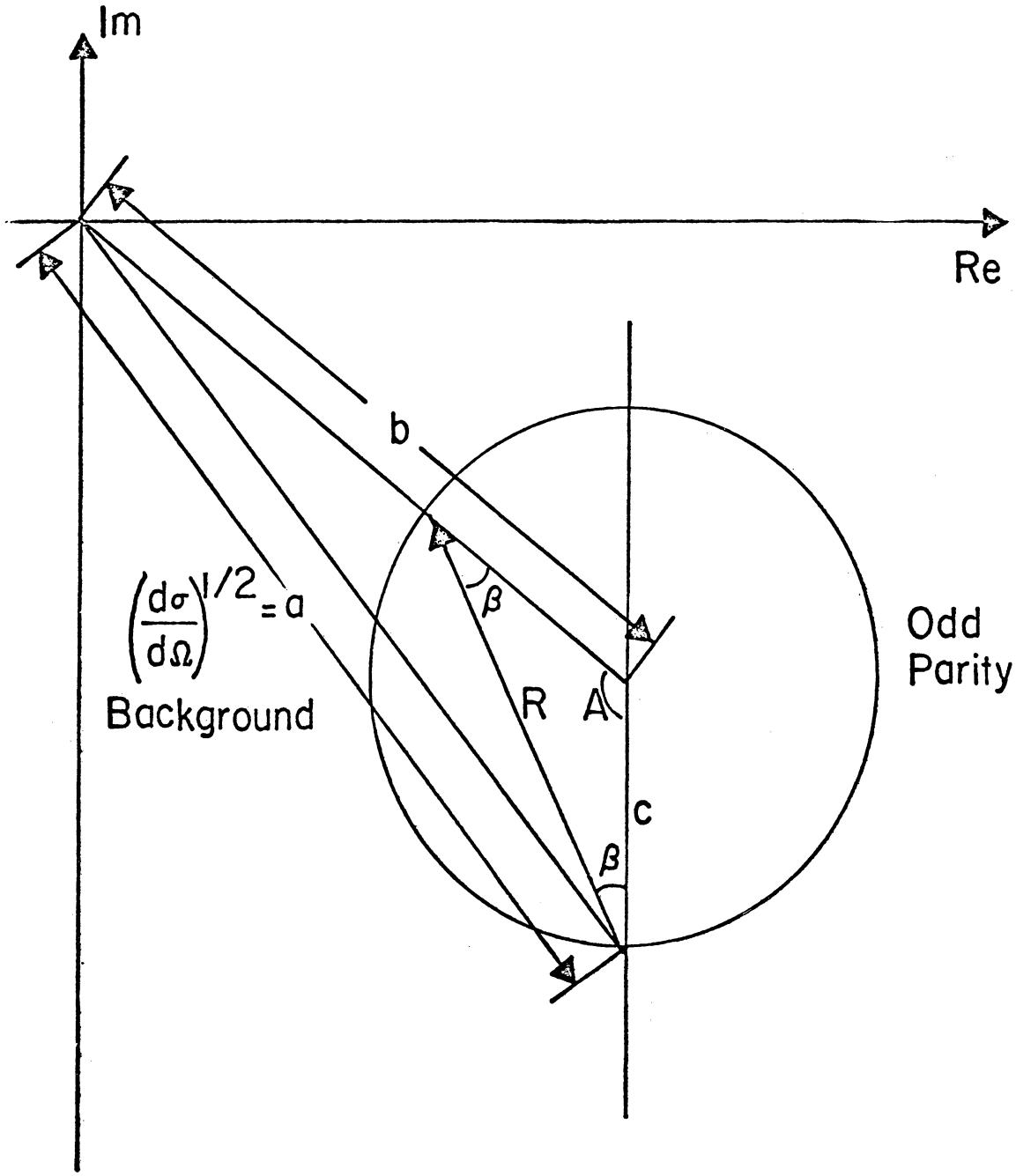

Figure 20. Destructive interference of background and resonance amplitudes.

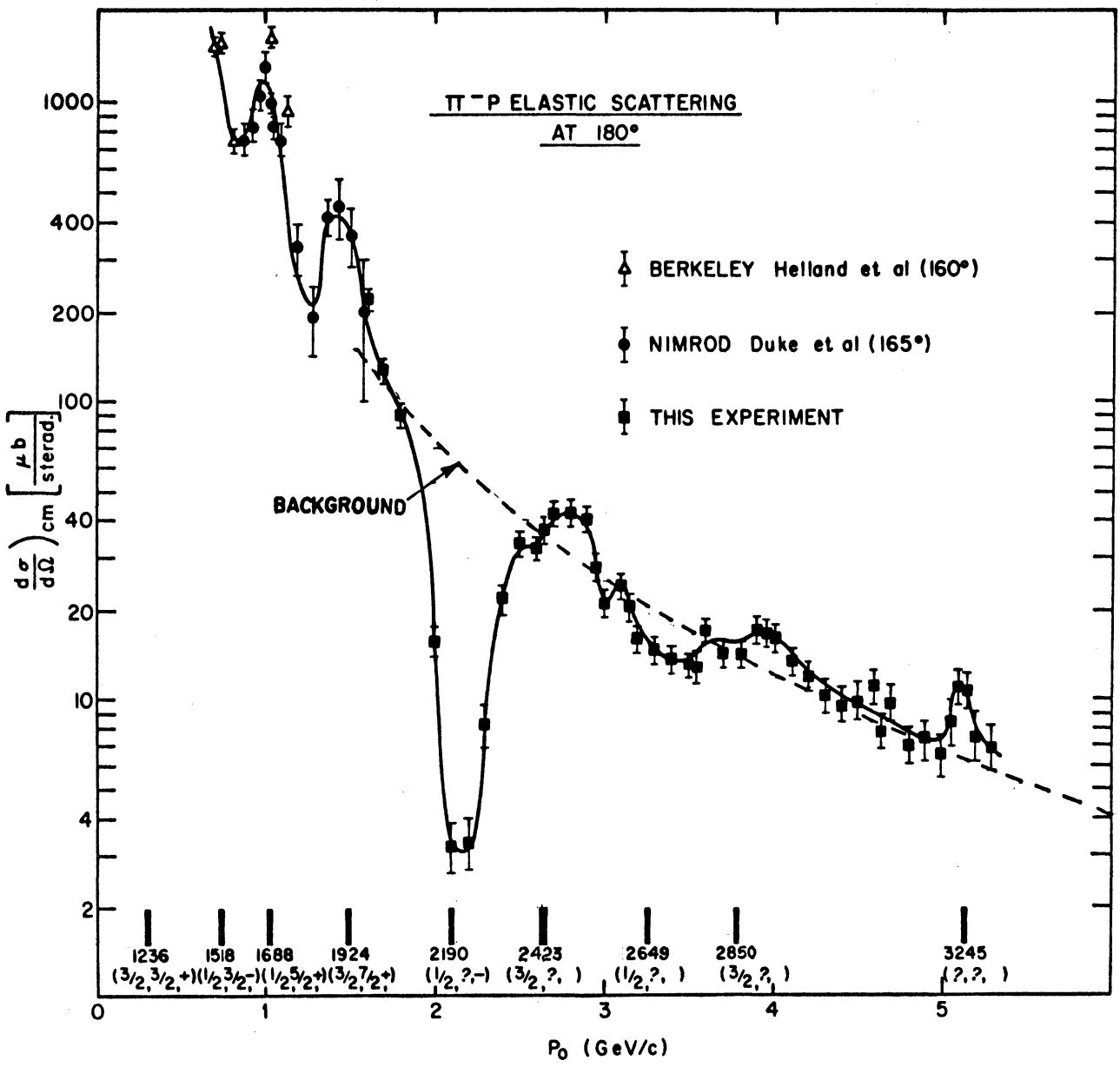

Figure 21. The assumed background cross section.

nances near the resonance energy. Also because the mimimum cross section near the 2190 resonance is at a greater energy than the 2190 resonance energy leads us to assume that the resonant amplitude is not in the third quadrant but that it lies in the fourth quadrant. The imaginary part of the background amplitude is negative and the real part is positive.

The parities and the quantitites X(J + 1/2) are listed in Table III.

TABLE III

THE EXPERIMENTAL PARITY AND X(J + 1/2) FOR THE N* RESONANCES

N*	I	J	P	Γ	X(J + 1/2)	X
2190	1/2	7/2	-	200	.46 ± 20%	.12 + 20%
2420	3/2		+	275	.31 ± 60%	
2650	1/2		-	300	.058 ± 70%	
2850	3/2		+	300	.12 ± 70%	
3245			+	35	$\frac{.073}{C}$ ± 80%	

The parities are determined by noting whether the resonance intereferes constructively or destructively with the background. Constructive interference indicates positive (+) parity while destructive intereference indicates negative (-) parity.

The quantities X(J + 1/2) for the resonances are determined from Figures 19 and 20 by trigonometry. For example, referring to Figure 20 we have by the Law of Cosines

$$a^2 = b^2 + c^2 - 2bc \cos A \qquad (30)$$

where

$$a = \left(\frac{d\sigma}{d\Omega}\right)^{1/2}_{\text{Background}}$$

$$b = \left(\frac{d\sigma}{d\Omega}\right)^{1/2}_{\text{Minimum}} + \frac{R_{\text{pure imaginary}}}{2}$$

$$c = \frac{R_{\text{pure imaginary}}}{2}$$

$$A = 2 \arctan \left(\frac{\text{Im } R}{\text{Re } R}\right)_{\substack{\text{At minimum} \\ \text{cross section}}}$$

$$= 2 \arctan \left(\frac{M\,\Gamma}{M^2 - S}\right)_{\substack{\text{At minimum} \\ \text{cross section}}}$$

$$\left|R_{\substack{\text{pure} \\ \text{imaginary}}}\right| = 19.73\ \lambda\ C\ (J + 1/2)\ X\ (\mu \text{ barns})^{1/2}.$$

From the above we solve for X(J + 1/2) consistent with the uncertainties in the values of the input parameters. These are shown in Table IV.

TABLE IV

INPUT PARAMETERS FOR THE DETERMINATION OF X(J + 1/2)

N*	$\left(\frac{d\sigma}{d\Omega}\right)$ Background	$\left(\frac{d\sigma}{d\Omega}\right)$ Maximum Minimum	Γ (Mev)	M (Mev)
2190	60 ± 15%	2.5 ± .5	200 ± 10	2190 ± 5
2420	28 ± 15%	42 ± 2	275 + 10	2423 ± 10
2650	19 ± 15%	14 ± 1	300 + 20	2649 ± 10
2850	12.5 ± 15%	17 ± 1	300 ± 20	2850 ± 12
3245	6.3 ± 15%	11 ± 1	50 ± 15	3230 ± 20

In many recent papers Barger and Cline[17-20] have given a phenomenological analysis of the cross section at 180° with a Reggized non-resonant background amplitude having both a real and imaginary part of the same order of magnitude. In the course of their calculations they have given parity, spin, and elasticity assignments to the resonances.

In a recent π^+p elastic scattering experiment near 180° by Dobrowolski, et al.,[23] the N* (2420) and N* (2850) were confirmed to have positive (+) parity.

APPENDIX

0° π^- PRODUCTION CROSS-SECTION

During the course of the experiment the 0° π^- production cross section on copper at 12.5 BeV/c was measured. For details see reference 21.

$d\sigma/d\Omega dP$ was calculated from

$$N_{\pi^-} = \Delta\Omega \Delta P T \frac{PtN}{A} \eta N_o \frac{d\sigma}{d\Omega dP}$$

where T = fraction of surviving pions at the H_2 target, N_o = number of calculating protons, and η = target efficiency factor. Other quantities are given in Table V.

In Table VI the zero degree π^- production by 12.5 GeV/c protons on copper is shown.

The following fluxes were obtained in the range 4.0 GeV/c to 5.2 GeV/c (Table VII). Since the target could not be moved further into the octant, we allowed the target to remain at the 4.0 BeV/c point which gave a range of production angles from 1/2° to 4° at the expense of the beam going off axis about 2 mrad. To stay on axis would have meant that the high momentum production angle would have been about 6-1/2°. The fluxes tabulated can be expected to vary about $\pm$ 15%

TABLE V

PROTON BEAM AND INTERNAL TARGET PARAMETERS

1. Beam Parameters

   a. $\Delta\Omega = 1.0 \times 10^{-4}$ sr

   b. $\frac{\Delta P}{P} = \pm 3/4\%$

   c. Beam length = 48 meters

2. Target Parameters

   a. 3.85" long x 1/8" x 1/8" target (90% copper, 10% aluminum)

   b. 0° production angle

   c. $\frac{PN}{A} = 8.06 \times 10^{23}$ cm^{-3}

3. Fluxes and Cross-Section

   a. Fluxes are for the average of several thousand pulses and the cross-section is normalized to a $(55 \pm 15)\%$ targeting efficiency.

   b. Above 3.5 GeV/c normalized to $(86 \pm 15)\%$ because of the addition of the beryllium lip on the target.

   c. Internal beam averaged $5 - 6 \times 10^{11}$ per pulse.

TABLE VI

ZERO DEGREE π^- PRODUCTION BY 12.5 GeV/c PROTONS ON COPPER

$P_{GeV/c}$	$N_\pi^-/10^{11}$, protons	$N_\pi^-/(GeV/c)/sr/circ.$, protons	$\frac{d\sigma}{d\Omega dp}$ (mb/sr/(GeV/c), nucleus
1.6	25×10^3	1.04×10^{-1}	398
1.7	33	1.30	478
1.8	33.3	1.23	440
2.0	40.6	1.35	445
2.1	40.7	1.29	419
2.2	41.3	1.25	400
2.3	43	1.25	392
2.5	46	1.23	375
2.6	45.5	1.17	351
2.7	46.4	1.15	340
2.8	42.9	1.02	299
2.9	47.1	1.08	309
3.0	47.4	1.05	300
3.1	43.1	0.93	261
3.2	45	0.94	264
3.3	45.8	0.93	257
3.4	43.7	0.86	238
3.5	44.9	0.86	235
3.5	67	1.28	235
3.6	62.1	1.15	212
3.7	66.2	1.19	216
3.8	65.9	1.16	210
3.9	61.0	1.04	188
4.0	64.0	1.07	191

TABLE VII

π^- FLUXES IN THE RANGE 4.0 GeV/c to 5.2 GeV/c.

$P_{GeV/c}$	$N_\pi-/10^{11}$ circ. protons	Production Angle	Off Axis Angle
4.0	64 x 10^3	0.5°	0.2 mrad
4.1	64	1.0°	
4.2	65	1.5°	
4.3	62	2.0°	
4.4	56	2.4°	
4.5	51	2.7°	
4.6	47	2.9°	
4.7	45	3.1°	
4.8	40	3.4°	
4.9	36	3.6°	
5.0	33	3.8°	2.0 mrad
5.1	30	3.85°	
5.2	29	3.9°	

BIBLIOGRAPHY

1. W. R. Frisken, A. L. Read, H. Ruderman, A. D. Krisch, J. Orear, R. Rubinstein, D. B. Scarl, and D. H. White, Phys. Rev. Letters 15, 313 (1965).

2. P. J. Duke, D. P. Jones, M.A.R. Kemp, P. G. Murphy, J. D. Prentice, J. J. Thresher, H. H. Atkinson, C. R. Cox, and K. S. Heard, Phys. Rev. Letters 15, 468 (1965); and private communication.

3. C. T. Coffin, N. Dikmen, L. Ettlinger, D. Meyer, A. Saulys, K. Terwilliger, and D. Williams, Phys. Rev. Letters 15, 838 (1965).

4. D. E. Damouth, L. W. Jones, and M. L. Perl, Phys. Rev. Letters 11, 287 (1963).

5. W. F. Baker, A. Lundby, et al., private communication.

6. M. L. Perl, Y. Y. Lee, and E. Marquit, Phys. Rev. 138, B707 (1965).

7. J. A. Helland, C. D. Wood, T. J. Devlin, D. E. Hagge, M. J. Longo, B. J. Moyer, and V. Perez-Mendez, Phys. Rev. 134, B1079 (1964).

8. S. W. Kormanyos, A. D. Krisch, J. R. O'Fallon, K. Ruddick, and L. G. Ratner, Rev. Letters 16, 709 (1966).

9. S. Penner, RSI, 32, 150 (1961).

10. D. V. Bugg, D. C. Salter, G. H. Stafford, R. F. George, K. F. Riley, and R. J. Tapper, Phys. Rev. 146, 980 (1966).

11. A Citron, W. Galbraith, T. F. Kycia, B. A. Leontic, R. H. Phillips, and A Rousset, Phys. Rev. Letters 13, 205 (1964).

12. J. Askin, T. Fassini, G. Fidecaro, Y. Goldschmidt-Clermont, N. H. Lipman, A. W. Merrison, and H. Paul, Nuovo Cimento 16, 490 (1960).

13. R. M. Heinz and M. H. Ross, Phys. Rev. Letters 14, 1091 (1965); and private communication.

14. W. Layson, Nuovo Cimento 27, 724 (1963); J. D. Jackson, ibid. 34, 1644 (1964).

15. Robert D. Tripp, Annual Review of Nuclear Science 15, 325 (1965).

16. A. H. Rosenfeld, A. Barbaro-Galtieri, W. H. Barkas, P. L. Bastien, J. Kirz, and M. Roos, Rev. Mod. Phys. 37, 663 (1965).

BIBLIOGRAPHY (Concluded)

17. V. Barger and D. Cline, Phys. Rev. Letters 16, 913 (1966).

18. V. Barger and D. Cline, Paper submitted to the XIIIth International Conference on High Energy Physics at Berkeley, 1966.

19. V. Barger and D. Cline, Phys. Letters 22, 666 (1966).

20. V. Barger and D. Cline, Fermion Regge Pole Model for the Structure of Pion-Nucleon Elastic Scattering in the Backward Hemisphere, to be published.

21. L. G. Ratner, $0°\pi^-$ production cross section on copper at 12.5 GeV/c and some π^- fluxes in the 17° beam line, Argonne National Laboratory internal report.

22. B. Jacobsohn and C. N. Yang, private communication.

23. T. Dobrowolski, et al., Paper submitted to the XIIIth International Conference on High Energy Physics at Berkeley, 1966.

Unclassified
Security Classification

DOCUMENT CONTROL DATA - R&D

(Security classification of title, body of abstract and indexing annotation must be entered when the overall report is classified)

1. ORIGINATING ACTIVITY (Corporate author)	2a. REPORT SECURITY CLASSIFICATION
The University of Michigan Department of Physics Ann Arbor, Michigan	Unclassified
	2b. GROUP

3. REPORT TITLE

π^-p Elastic Scattering at 180 Degrees from 1.6 to 5.3 GeV/c

4. DESCRIPTIVE NOTES (Type of report and inclusive dates)

Technical Report

5. AUTHOR(S) (Last name, first name, initial)

Kormanyos, Stephen W.

6. REPORT DATE	7a. TOTAL NO. OF PAGES	7b. NO. OF REFS
April 1967	76	23

8a. CONTRACT OR GRANT NO.	9a. ORIGINATOR'S REPORT NUMBER(S)
Nonr-1224(23)	03106-28-T
b. PROJECT NO. NR-022-274	
c.	9b. OTHER REPORT NO(S) (Any other numbers that may be assigned this report) Technical Report No. 28
d.	

10. AVAILABILITY/LIMITATION NOTICES

Distribution of this document is unlimited.

11. SUPPLEMENTARY NOTES	12. SPONSORING MILITARY ACTIVITY
	Department of the Navy Office of Naval Research Washington, D.C.

13. ABSTRACT

We have measured the differential cross section for π^-p elastic scattering at 180° in steps of 0.10 GeV/c or less in the region from 1.6 to 5.3 GeV/c.

There is considerable structure in the cross section. This may be interpreted as an interference effect between the resonance amplitude and the non-resonant or background amplitude.

There is a dramatic destructive interference at P_o = 2.15 GeV/c which is quite interesting as the cross section drops almost two orders of magnitude in this region.

Another interesting feature of the experiment is the large narrow peak in the cross section at P_o = 5.12 GeV/c. We believe that this is firm evidence for the existence of a nucleon resonance with a mass of (3245 $\pm$ 10) MeV. This N* (3245) has a full width at half-maximum of less than 35 MeV. The width of the resonance is about 1% of its mass.

Parities and the quantity X(J + 1/2) are given for various N* resonances where X is the elasticity and J is the spin of the resonance.

DD FORM 1 JAN 64 1473

Unclassified
Security Classification

14. KEY WORDS	LINK A		LINK B		LINK C	
	ROLE	WT	ROLE	WT	ROLE	WT

INSTRUCTIONS

1. ORIGINATING ACTIVITY: Enter the name and address of the contractor, subcontractor, grantee, Department of Defense activity or other organization *(corporate author)* issuing the report.

2a. REPORT SECURITY CLASSIFICATION: Enter the overall security classification of the report. Indicate whether "Restricted Data" is included. Marking is to be in accordance with appropriate security regulations.

2b. GROUP: Automatic downgrading is specified in DoD Directive 5200.10 and Armed Forces Industrial Manual. Enter the group number. Also, when applicable, show that optional markings have been used for Group 3 and Group 4 as authorized.

3. REPORT TITLE: Enter the complete report title in all capital letters. Titles in all cases should be unclassified. If a meaningful title cannot be selected without classification, show title classification in all capitals in parenthesis immediately following the title.

4. DESCRIPTIVE NOTES: If appropriate, enter the type of report, e.g., interim, progress, summary, annual, or final. Give the inclusive dates when a specific reporting period is covered.

5. AUTHOR(S): Enter the name(s) of author(s) as shown on or in the report. Enter last name, first name, middle initial. If military, show rank and branch of service. The name of the principal author is an absolute minimum requirement.

6. REPORT DATE: Enter the date of the report as day, month, year; or month, year. If more than one date appears on the report, use date of publication.

7a. TOTAL NUMBER OF PAGES: The total page count should follow normal pagination procedures, i.e., enter the number of pages containing information.

7b. NUMBER OF REFERENCES: Enter the total number of references cited in the report.

8a. CONTRACT OR GRANT NUMBER: If appropriate, enter the applicable number of the contract or grant under which the report was written.

8b, 8c, & 8d. PROJECT NUMBER: Enter the appropriate military department identification, such as project number, subproject number, system numbers, task number, etc.

9a. ORIGINATOR'S REPORT NUMBER(S): Enter the official report number by which the document will be identified and controlled by the originating activity. This number must be unique to this report.

9b. OTHER REPORT NUMBER(S): If the report has been assigned any other report numbers *(either by the originator or by the sponsor)*, also enter this number(s).

10. AVAILABILITY/LIMITATION NOTICES: Enter any limitations on further dissemination of the report, other than those imposed by security classification, using standard statements such as:

(1) "Qualified requesters may obtain copies of this report from DDC."

(2) "Foreign announcement and dissemination of this report by DDC is not authorized."

(3) "U. S. Government agencies may obtain copies of this report directly from DDC. Other qualified DDC users shall request through _____."

(4) "U. S. military agencies may obtain copies of this report directly from DDC. Other qualified users shall request through _____."

(5) "All distribution of this report is controlled. Qualified DDC users shall request through _____."

If the report has been furnished to the Office of Technical Services, Department of Commerce, for sale to the public, indicate this fact and enter the price, if known.

11. SUPPLEMENTARY NOTES: Use for additional explanatory notes.

12. SPONSORING MILITARY ACTIVITY: Enter the name of the departmental project office or laboratory sponsoring *(paying for)* the research and development. Include address.

13. ABSTRACT: Enter an abstract giving a brief and factual summary of the document indicative of the report, even though it may also appear elsewhere in the body of the technical report. If additional space is required, a continuation sheet shall be attached.

It is highly desirable that the abstract of classified reports be unclassified. Each paragraph of the abstract shall end with an indication of the military security classification of the information in the paragraph, represented as *(TS), (S), (C), or (U)*.

There is no limitation on the length of the abstract. However, the suggested length is from 150 to 225 words.

14. KEY WORDS: Key words are technically meaningful terms or short phrases that characterize a report and may be used as index entries for cataloging the report. Key words must be selected so that no security classification is required. Identifiers, such as equipment model designation, trade name, military project code name, geographic location, may be used as key words but will be followed by an indication of technical context. The assignment of links, rules, and weights is optional.